



Instituto Superior Técnico

Universidade de Lisboa

Integrated Masters in Aerospace Engineering

Aerospace Design - Group 1

Urban Air Mobility

Ana Veiga, 86608
André Rocha, 86612
Francisco Sargento, 86629
Hugo Faustino, 86636
Miguel Morgado, 86668
Olívia Pinto, 86671
Sara Pessoa, 83731

Coordinator: Professor Afzal Suleman
Assistant Coordinator: Professor Frederico Afonso

January 2021

Abstract

In the present project, an hybrid-electric Vertical Take-Off and Landing Aircraft for Urban Air Mobility that will enter in service in 2030 is designed. After several concepts are presented to execute a proposed mission profile, a careful study of the main components of the aircraft, its environmental impact and a cost analysis are performed, in order to obtain a feasible and affordable aircraft.

Contents

1	Introduction	1
1.1	Motivation and Objectives	1
1.2	Design Requirements	1
1.3	Market Research	2
1.3.1	Conventional Aircraft	2
1.3.2	Aurora Boeing Personal Air Vehicle	2
1.3.3	Airbus CityAirbus	3
1.3.4	Joby Aviation's Aircraft	3
1.3.5	Lilium Jet	4
1.4	Mission Profile	5
2	Concept Selection	7
2.1	Analytic Hierarchy Process	9
3	Aircraft Sizing	10
3.1	Methodology	10
3.2	Parametric Studies	10
3.2.1	Mission Parameters	10
3.2.2	Forward Flight	12
3.3	Vertical Flight	13
3.4	Design Point	14
4	Wing Design	15
4.1	Airfoil Selection	15
4.2	3D Wing Design	17
4.2.1	Aspect Ratio	17
4.2.2	Sweep Angle	17
4.2.3	Taper Ratio	17
4.3	Lift and Drag Estimation	17
5	Tail design	19
5.1	Tail Configuration	19
5.2	Airfoil selection	20
5.3	Sizing	20
6	Fuselage	22
6.1	Internal Dimensions	22
6.1.1	Standard Air Taxi	22
6.1.2	Aeromedical	23
6.1.3	Cargo	23
6.2	External Dimensions	24
6.3	Landing Gear	25
6.4	Other Structural Components	26
7	Structural Design	27
7.1	Flight Envelope	27
7.2	Shear stress and bending moment	28
7.2.1	Wing	28
7.2.2	Fuselage	30
7.3	Material Selection	33

8 Static Stability	34
8.1 Longitudinal stability	34
8.1.1 Procedure	35
8.2 Lateral Stability	36
8.3 Directional Stability	37
9 Propulsion	39
9.1 Vertical Flight	39
9.1.1 Electric Propulsion	39
9.1.2 Rotor Design	39
9.2 Forward Flight	40
9.2.1 ICE Propulsion	40
9.2.2 Propeller Design	41
9.3 Propulsive Architecture	42
10 Emissions	43
10.1 Noise	43
10.2 Pollutant Emissions	43
11 Cost Analysis	45
11.1 Development, testing, evaluation and production	45
11.1.1 Development, Testing and Evaluation	46
11.1.2 Acquisition/Production	47
11.2 Operations and Maintenance	47
11.3 Research cost	49
11.4 Total top-down approximate cost	49
12 CAD Model	50
13 Conclusion	51

List of Figures

1	2
2	Aurora Boeing Personal Air Vehicle and its specifications. [4]	3
3	Airbus CityAirbus and its specifications. [6]	3
4	Joby Aviation's Aircraft and its specifications. [7]	4
5	Lilium Jet and its specifications. [8]	4
6	Mission path	5
7	Mission profile	6
8	Chosen sketches.	7
9	MTOW with vertical take off speed and height	11
10	Cruise speed constraints and final design point	12
11	Lift to Drag ratio with Aspect ratio and mean chord	13
12	Design point	14
13	NACA 4412	15
14	NACA 4418	15
15	C_l with α for the NACA 4412 and NACA 4418 airfoils	16
16	C_l/C_d with α for the NACA 4412 and NACA 4418 airfoils	16
17	H-tail configuration as viewed on the concept CAD.	20
18	Air Taxi configuration.	22
19	Cross section of the cabin	23
20	Air ambulance configuration.	23
21	Cargo configuration.	23
22	Fuselage lenght vs W_0 (imperial units) [10]	24
23	Fineness ratio in subsonic vs C_{D_0}	24
24	Fuselage length ratios [11]	25
25	Wheel sizing [10]	25
26	Statistical gust velocities [9]	27
27	Combined V-n diagram	28
28	Distribution of loads across the wing	29
29	Shear stress (a) and bending moment (b) along half the wingspan.	29
30	Shear stress (a) and bending moment (b) along the fuselage for the air taxi configuration.	31
31	Shear stress (a) and bending moment (b) along the fuselage for the air ambulance configuration.	32
32	Shear stress (a) and bending moment (b) along the fuselage for the cargo configuration.	32
33	Illustration showing the aircraft axes and directions [9]	34
34	Illustration showing forces and distances on a conventional aircraft [17]	35
35	Variation of the downwash factor [17]	35
36	Lateral aircraft arrangement	36
37	Sample propeller efficiency for forward flight (three blade propeller) [9]	42
38	Propulsive architecture used in vertical flight.	42
39	Propulsive architecture used in forward flight.	42
40	Distribution of the total CO_2 equivalent emissions by source for the lifetime of each UAM aircraft.	44
41	Hourly wage empirical extrapolation, based on the value of 1998 USD [17]	45
42	Total top down cost pie chart	49
43	CAD image of the final aircraft design (side view)	50
44	CAD image of the final aircraft design (front view)	50
45	CAD image of the final aircraft design (top view)	51
46	CAD image of the final aircraft design (isometric view)	51

List of Tables

1	Specifications of the most used aircraft in the Vancouver area.	2
2	Tail geometric parameters.	21
3	Passengers' seats and aisle dimensions	22
4	Maximum values for shear force and bending moment in the wing.	30
5	Configuration specific aircraft components.	30
6	General aircraft components.	31
7	Maximum absolute values for shear force and bending moment in the fuselage. .	32
8	<i>MagniX magniDrive</i> electric motor specifications [19].	39
9	Market study for electric motors [19].	39
10	Rotor characteristics.	40
11	Cruise conditions.	41
12	Market study for ICE propulsion [20].	41
13	Rolls-Royce M250-C28B motor specifications [20].	41
14	Obtained values for hourly wages for the different categories	46
15	Empirical relation for the work hours needed	46
16	Top down cost of the DT&E phase	47
17	Top down cost of the Acquisition/Production phase	47
18	Constants used for the O&M Cost calculation	48
19	Top down costs for O&M phase for ten years of operation	48
20	Top down cost overview	49

1 Introduction

1.1 Motivation and Objectives

The aim of the current project is to design an all-electric or hybrid-electric Vertical Take-Off and Landing (VTOL) Aircraft for Urban Air Mobility (UAM) that will be able to enter in service in 2030.

Demand for VTOL aircraft is increasing, mainly due to its versatility in operation, since only a small helipad is required for take-off and landing, thus excluding the need for runways during these procedures. This allows VTOL to operate on missions with difficult access, reducing times for civil protection operations and for cargo delivery.

Taking all the above into consideration, it is understandable that the use of VTOL aircraft is increasing for the emerging aviation segment of UAM, with several applications demanded, in which the “air-taxi” is included, since this means of transportation allows the avoidance of traffic in highly congested cities. There are other applications which use VTOL, such as Aeromedical, permitting a response in smaller times, and Cargo, permitting the access to locations of difficult access by land.

Although existent helicopters can carry out the missions presented, since UAM operations are located in large urban areas, it is compulsive that lower noise and pollutant emissions signatures than those of conventional helicopters are sought, characteristics demanded from a new VTOL aircraft generation that is currently being developed.

This report starts by analysing the requirements imposed on the project, comparing several aircrafts both currently present in the market and proposed in the literature. Having those into consideration, several sketches are presented, from which one is selected.

Regarding the topics exposed, the current section introduces the General Requirements of the intended design, overviews the present competition available on the market and describes the Mission Profile proposed. The second chapter contemplates both the Concept Selection and the Analytic Hierarchy Process, used to more easily select the chosen concept. The following one concerns the Aircraft Sizing, taking into account the Methodology proposed while covering the Parametric Studies done to select the initial design parameters. The fourth one highlights the Wing Design and the fifth the Tail Design. The Fuselage is studied in the sixth section and the Structural Design analysed in the seventh. In the eighth chapter one studies the Static Stability and Propulsion is examined in the following one. A study on the Emissions, taking into account the environmental impact, is made in the tenth section and the Cost Analysis concludes the research in the eleventh chapter.

1.2 Design Requirements

When designing a new aircraft, the design requirements are the first aspect to take into consideration.

In the request proposal, the following design requirements were stated for the aircraft:

- Payload of 600 kg;
- Operational radius of 300 km;
- Maximum take-off mass lower than 3,000 kg;
- Cruise speed within 100 and 200 kts;
- Nominal cruise altitude of 1,500 m AGL;
- Service ceiling not exceeding 3,000 m;
- Divert range of 10 km;

- Footprint lower than 15 m (helipad dimensions);
- Operating temperature range within -40°C and 50°C;
- 20 minutes of reserve energy.

1.3 Market Research

The first important step in any design project is to perform a market study, searching for direct competitors, such as already existing and operating aircraft that perform a similar mission, as well as the state-of-the-art in VTOL and UAM vehicles.

1.3.1 Conventional Aircraft

Since the decision of entering the market in the Vancouver Island area was made, it is pertinent to provide an overview of which services are available in the present moment. There are several airlines (Air Canada, WestJet and Pacific Coastal) doing the Vancouver-Victoria route, mostly using larger aircraft, such as De Havilland Dash 8-400. Besides that, two smaller companies (Harbour Air and Helijet) offer the same service, using seaplanes and helicopters, presenting the advantage of flying from and to downtown instead of the airport. Images and specifications of the most used aircraft are present in Figure 1 and Table 1. [1-3]



Figure 1

Table 1: Specifications of the most used aircraft in the Vancouver area.

	De Havilland Dash 8-400	De Havilland DHC-3	Bell LongRanger 206L3
MTOW	27 987 kg	3629 kg	1882 kg
Cruise speed	360 kt	120 kt	104 kt
Range	2522 km	1540 km	515 km
Passengers	78	11	5
Flight duration	30 min	35 min	35 min
Price	\$300	\$200	\$300

1.3.2 Aurora Boeing Personal Air Vehicle

Aurora Flight Sciences is a subsidiary of Boeing, which is designing an electric VTOL prototype. Firstly, the concept was tested on a 1:10 model, followed by a 1:4 scale concept aircraft to be used in some flight tests.

The model consists of a three-surface aircraft that has twin booms, each supporting four rotors slightly angled alternatively outward and inwards, a pusher propeller and the rear wing, which has vertical surfaces at each end.



(a) Aurora Boeing Personal Air Vehicle.

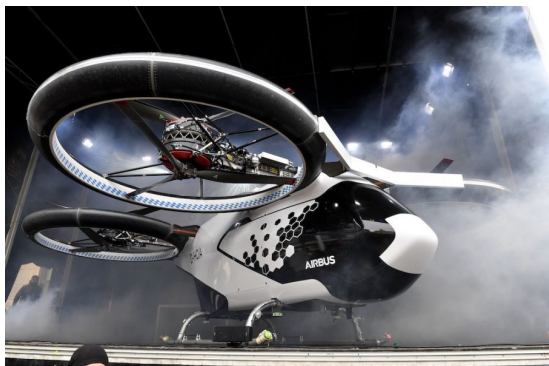
Capacity	2 pax (225 kg payload)
Cruise Speed	97 knots
Range	80 km
MTOW	800 kg
Propellers	5-bladed
Length	9.14 m
Wingspan	8.53 m
Crew	None (autopilot)
Energy Source	All Electric
Development Status	Introduction planned for 2024

(b) Aurora Boeing Personal Air Vehicle Specifications.

Figure 2: Aurora Boeing Personal Air Vehicle and its specifications. [4]

1.3.3 Airbus CityAirbus

Currently in development by Airbus Helicopters, CityAirbus is an all-electric VTOL prototype which could provide transportation for up to four people and avoid traffic congestion inside metropolitan areas, serving as an air taxi. The first flight of a prototype was done in Germany on the 3rd of May, 2019. It was just a tethered hover, a few meters off the ground. [5]



(a) CityAirbus being presented in Ingolstadt, Germany.

Capacity	4 pax (250 kg payload)
Cruise Speed	65 knots
Endurance	15 min
Range	<30 km
MTOW	2200 kg
Rotors	8 ducted fans, 100 kW each
Energy Source	All Electric
Propellers	eight 3-bladed, 2.8 m in diameter
Length	8m
Wingspan	8 m
Crew	Can fly with or without a pilot
Development Status	Commercialization planned for 2023

(b) CityAirbus Specifications.

Figure 3: Airbus CityAirbus and its specifications. [6]

1.3.4 Joby Aviation's Aircraft

This nameless aircraft is being developed by Joby Aviation in partnership with Uber and Toyota, and aims to provide a fully electric aircraft for taxi service for four passengers by the end of 2023. Due to being fully electric, the aircraft produces zero carbon emissions and is nearly silent during cruise flight. When taking off, it is hundred times more silent than a conventional aircraft.

Joby Aviation has already raised \$590 million to finance their air taxi service launch.



(a) Joby Aviation's Aircraft.

Capacity	4 pax
Cruise Speed	170 kts
Range	240 km
MTOW	—
Propellers	6 Tilt motors
Length	—
Wingspan	—
Crew	1 pilot
Energy Source	All electric
Development Status	Expected launch in 2023

(b) Joby Aviation's Aircraft Specifications.

Figure 4: Joby Aviation's Aircraft and its specifications. [7]

1.3.5 Lilium Jet

The Lilium Jet is a proposed German VTOL personal air vehicle designed by Lilium GmbH. The Lilium Jet five-seater prototype first flew in May 2019.

Lilium claims that its jet is capable of completing much longer journeys than the majority of its competitors, thanks, in part, to its fixed-wing design. Moreover, its 36 electric motors provide near-instantaneous thrust in almost any direction, so that control surfaces, such as rudders, ailerons or a tail, are not required.



(a) Lilium Jet.

Capacity	4 pax
Cruise Speed	160 kts
Range	300 km
MTOW	—
Propellers	36 single-stage electric motors
Length	—
Wingspan	—
Crew	1 pilot
Energy Source	All electric
Development Status	Expected launch in 2025

(b) Lilium Jet Specifications.

Figure 5: Lilium Jet and its specifications. [8]

1.4 Mission Profile

The decision of operating in the Vancouver area was made since the current services are limited and it would be beneficial the existence of a versatile aircraft such as the one developed in this project, that can perform passenger, ambulance and cargo missions. For reference, a possible mission path would be between the cities of Vancouver, Nanaimo and Victoria. Due to restrictions in battery weight, the best option was to perform only two segments in one mission, making a total distance of 156 km. The approximate duration of each segment is expected to be 35 min, which is similar to the flight duration of the conventional aircraft presented in the previous section.

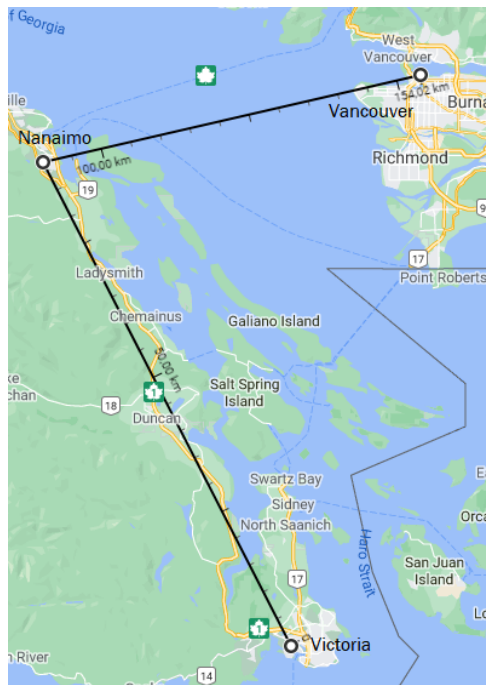


Figure 6: Mission path

The mission profile's plot is shown below. It begins with a vertical take-off at a constant velocity of 4 m/s to around 150 m. Once that's finished, the aircraft transitions to its horizontal mode and start climbing to the nominal cruise height of 1500 m. The cruise is the most time consuming part of the mission, taking roughly 20 minutes. Once the aircraft has reached its final destination, it descends to 150 m, from where, it vertically lands at 4 m/s.

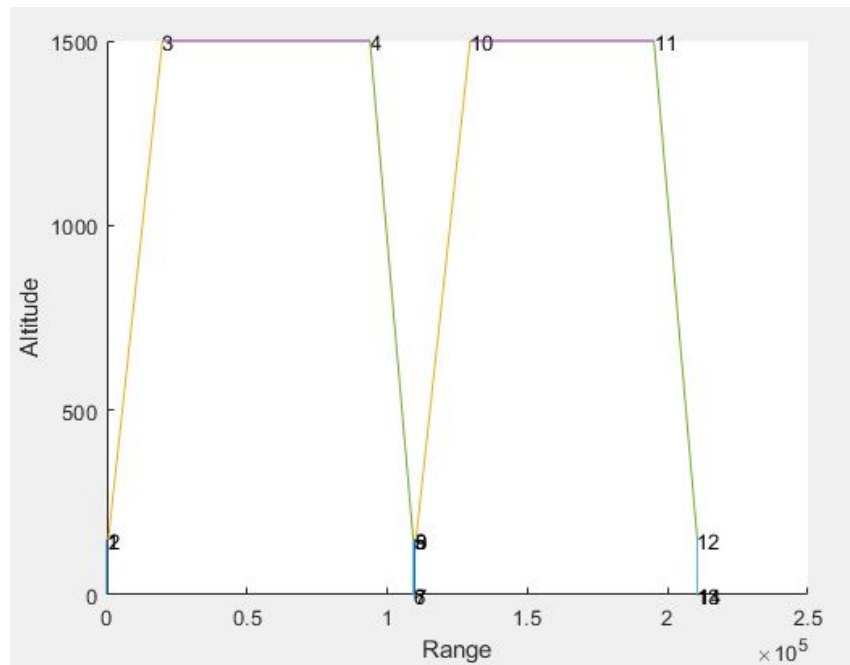
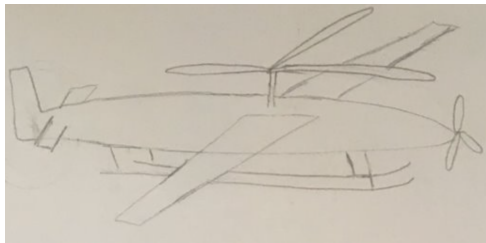


Figure 7: Mission profile

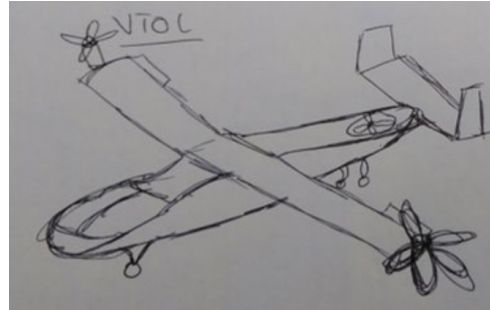
2 Concept Selection

Given the objectives and the considered mission profile, the team sketched several concepts that fulfilled the set of design requirements mentioned in section 1.2. A total of fourteen different initial ideas were grouped together into categories. These categories were: Compound Helicopters, Tilt-rotor Aircraft, Fixed Wing VTOL Aircraft and Quadcopters.

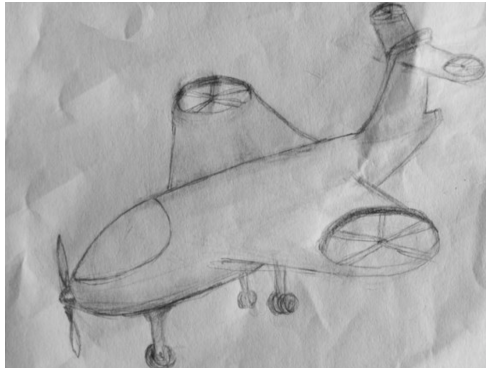
From the several concepts sketched by us, we analysed the benefits and drawbacks of the ones in the following figure:



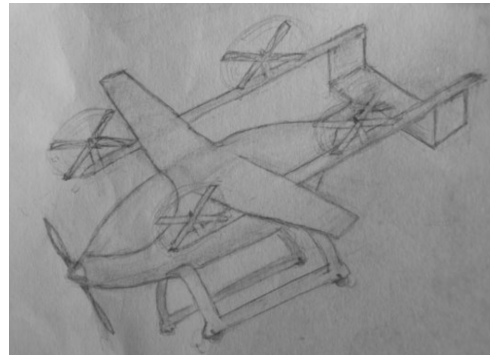
(a) Concept 1



(b) Concept 2



(c) Concept 3



(d) Concept 4

Figure 8: Chosen sketches.

Concept 1 - Compound Helicopter

Advantages

- Mechanically easy concept;
- Forward flight.

Disadvantages

- Drag;
- Lateral drift.

Concept 2 - Tilt-rotor

Advantages

- Good VTOL and cruise performance;
- Simple.

Disadvantages

- Takes few passengers.

Concept 3 - Fixed Wing VTOLAdvantages

- Simple;
- Aesthetically pleasing.

Disadvantages

- Drag and low lift from wing holes.

Concept 4 - Fixed Wing QuadcopterAdvantages

- No rotating structures or propellers;
- + VTOL stability.

Disadvantages

- Many propellers, noise;
- Drag.

In order to appraise the most adequate aircraft, it was decided to use the Analytic Hierarchy Process (AHP). This process is used in analytic decision making to choose the best option presented among a group, attending to the chosen criteria.

The following parameters were selected, according to the mission requirements:

- construction/maintenance
 - costs
 - structural
 - integrity
 - maintenance
 - reliability/safety
- operation
 - in flight
 - * noise pollution/acoustics
 - * stability
 - * aerodynamics (L/D)
 - * controllability
 - * versatility
 - * performance VTOL
 - * performance forward flight
 - on ground
- power plant
 - max power installed
 - pollutant emissions
- innovation

The second step to take into account in the AHP will be the attribution of a certain importance level to each of the parameters presented. The scale chosen varies from 1 to 9, where 1 represents two parameters that contribute equally to the aim of the project and 9 means that the evidence favouring one parameter when compared to the other is of the highest possible order of affirmation.

It is still necessary to attribute a classification for each of the different configurations in their performance on the several chosen parameters. It was selected a scale going from 1 to 9, where 1 represents a lack of capability on the performance of a certain parameter by the design, whereas 9 represents an excellent performance level on the part on the parameter chosen.

2.1 Analytic Hierarchy Process

The parameters have the following order of importance (from the most to the least important): construction/maintenance and operation, power plant and innovation. It is of the most importance for the aircraft to have a good performance during the operation and for it to be well constructed and of easy maintenance. It should also be reliable and attention should be given to the level of pollutant emissions, especially since it will be operating nearby urban areas.

Within the construction/maintenance parameter, the following sub-parameters are ordered from the most to the least important, according to our choosing: maintenance, structural integrity and costs, and reliability/safety. It is of extreme importance that the aircraft be economically maintained in order to keep functioning according to what is expected. The structural integrity field is also important in order to ensure that the structure is fit for its normal operational conditions and even when the conditions presented exceed the ones predicted during its normal design.

Within the operation parameter, the sub-parameter in flight was considered more important than the operation on ground, since the majority of the operation will be ‘in flight’.

When it comes to the flight operation, the most important topic will be the forward performance, since it consists of most of the time of the mission. This sub-parameter is followed by stability and the noise pollution/acoustics comes in third place in terms of importance in this parameter, which is important considering the aircraft will also be flying in urban areas, where noise regulations are present. The VTOL performance is another aspect to take into consideration, although, since it comprises such a small time of the mission, it will have a much smaller weight in terms of importance, when compared, for instance, to the forward flight performance. The least important aspects in this parameter are the controllability and versatility of the aircraft; since the aircraft presented is not made for military use, its stability will be more important than its controllability, when performing the mission.

Concerning the power plant parameter, the pollutant emissions are considered more important than the maximum power installed, since the aircraft will be flying over urban areas, where the pollutant emissions are restricted.

3 Aircraft Sizing

This section will present and explain the sizing the most simple elements and parameters of our aircraft. It will start by explaining some of the unique challenges faced by VTOL airplane designers, then the design methodology will be presented, as well as some parametric studies concerning the complex interaction between the different mission, horizontal and vertical flight parameters. Finally, the design space and points will be shown and explained.

While conventional aircraft sizing is far from straightforward, the sheer scarcity, complexity and novelty of modern eVTOL airplanes makes this latter kind of aircraft design even more complex and convoluted. Despite having some military applications, and some more recent privately backed VTOL designs, there is still a dire scarcity of literature and general resources regarding VTOL aircraft design, specially when compared to the vast ocean of knowledge available regarding conventional aircraft design. To make matters worse, most eVTOL designs are so recent that its companies have not made public most of their design methodology.

Regardless, the main goals and methods of eVTOL aircraft design have much in common with its more conventional cousins, and some concepts like power loading and disk loading can be borrowed from them.

3.1 Methodology

From the very start of the design process, the main objectives were laid out, and were then used as the criteria to evaluate each design iteration and alteration:

- **Low MTOW**, which makes the design more efficient, and helps tremendously in most other aspects of aircraft design: for example, a lighter plane will need less power.
- **Low cruise speed**, since the nominal cruise altitude is low, and a higher cruise speed would result in more stringent power constraints for just a modest decrease in travel time. In such a way, range and operational potential were prioritized, instead of speed.
- **Minimal complexity**, to minimize costs and streamline the development of the aircraft. It may seem contradictory to prioritize low complexity in an hybrid design that is by its very nature complex, however, one can use this criterion when choosing a simple and efficient propulsion, avoiding tilt rotors and wings.
- **Mission flexibility**, which makes the aircraft more useful and attractive from a client's point of view. Thus, this airplane was designed to perform several stops before needing to recharge its batteries.

To study the interaction between all the different mission and aircraft parameters, and its following of the initial goals, a *matlab* tool developed by Mário Brás and Ricardo Marques was used: the *aircraft-design-tool* is an open source *matlab* tool to perform aircraft sizing. Its reference can be consulted in the bibliography section. This tool supports eVTOL designs and is easy to use, making it invaluable in performing different design iterations.

To optimize the mission profile and the aircraft design, this tool was used to perform parametric studies of several parameters, which will be explained on the next subsection.

3.2 Parametric Studies

3.2.1 Mission Parameters

In the next few paragraphs, there will be an explanation of how and why the values for some of a typical mission's parameters were selected. While the aircraft can follow several mission profiles, depending on the situation, its design was optimized around a particular set

of mission parameters, and, by the same token, the aircraft's design was optimized around this same mission profile.

- **Vertical Take off speed and transition altitude:** The vertical take off and landing segments are the only ones where the batteries and rotors are used, therefore it is of the utmost importance that this segment be optimized. A high vertical take off speed dramatically increases the vertical power requirement, which in turn increases cost, mass and complexity, and, on the other hand, a low take off speed increases the time that the batteries have to be used, and hence, their mass. Consequently, this speed should be as high as the selected vertical propulsion allows, so as not to waste the potential of the engine and rotors installed. The vertical segment's height is also extremely relevant: a high transition altitude tremendously increases the battery's mass, yet, it can not be lower than 100 meters, specially in an urban environment, dotted with high rise buildings. This aircraft is designed to transition from electric to ICE propulsion from 150 to 400 meters, while being able to do so 3 times before recharging.

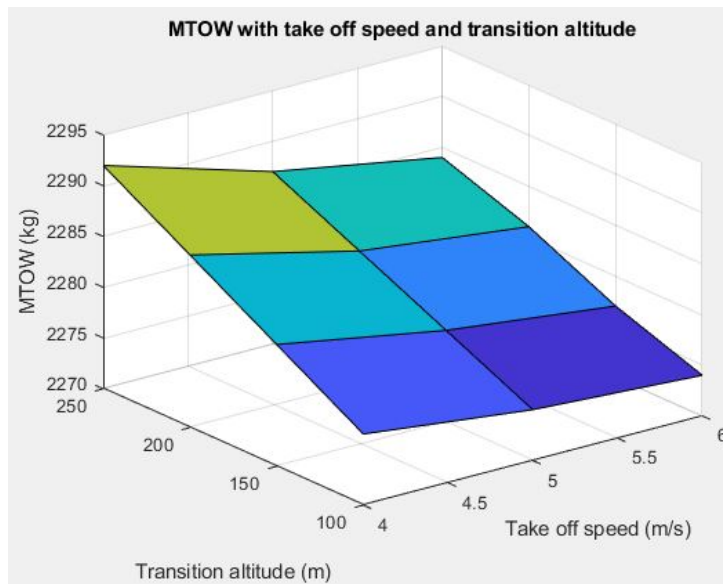


Figure 9: MTOW with vertical take off speed and height

Figure 9 shows how the vertical take off parameters influence MTOW: it decreases with the take off speed, and increases with the transition altitude. Both these observations are obvious, be it as it may, it is important to study how heavier the aircraft gets when it is submitted to tougher mission parameters.

One relevant conclusion to take from this graph is that a vertical take off from sea level to 250 metres only adds 20 kg of to the aircraft's mass, meaning that it is capable of longer vertical segments without sacrificing forward performance, or the number of stops performed per mission. At first glance, a longer take off may seem pointless, however, the longer it is, the safer and easier the transition segment will be. Additionally, some clients may require longer vertical segments, depending on the weather, potential obstacles on the flight path, or even due to an increased mass.

- **Climb angle:** In general, an aircraft with more power installed will be able to pull off steeper climbs, decreasing the climb time, notwithstanding, since the nominal cruise height is only 1500 meters, a large climb angle and speed is not of paramount importance. Hence, just as we optimized the vertical take off parameters around the vertical propulsion installed, we also optimized the climb parameters around the horizontal power installed, using the design point and the climb constraint curve.

- **Cruise velocity:** The higher the cruise velocity, the higher the horizontal power requirement. Moreover, urban air mobility does not require high cruise speeds, since only about half of each trip between two stops is occupied by a cruise segment, so having a high cruise speed aircraft is not as valuable as having a more efficient and cheaper low speed model. However, navigating at low speed is also dangerous, since the airplane can approach the stall speed, which brings a lot of instability issues. Thus, a combination of design point and flight envelope plots was used to determine a good cruise speed for the aircraft.

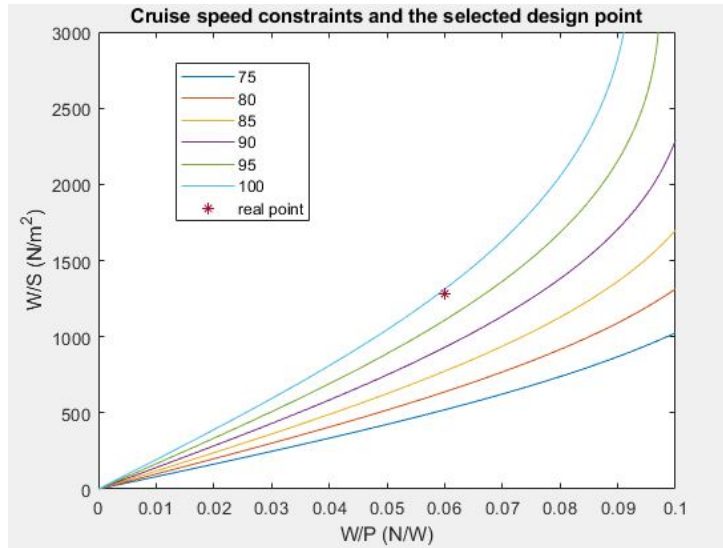


Figure 10: Cruise speed constraints and final design point

Figure 10 shows the cruise speed constraints imposed by a range of cruise velocities: an higher v_c translates to a more stringent horizontal mode constraint. This plot also depicts the selected horizontal design point as a red dot.

The key conclusion to take is that whilst the aircraft was designed to operate at $85m/s$, it is also able to fly well above its nominal cruise speed. This allows the aircraft to fly at a large range of speeds, and to carry even heavier payloads, granting a high degree of flexibility to pilots and clients alike.

3.2.2 Forward Flight

- **Aspect ratio:** A high aspect ratio of at least 7.5 is often used in most modern aircraft, since it is often the most efficient way of increasing the lift to drag ratio, and hence cruise performance. Increasing AR, for a constant mean chord, has few drawbacks, therefore, early on the design process it was decided to keep it high, however, increasing it also means increasing the wing's span, which has some cons. A longer wing will have to support higher loads, and will thus have to be heavier, so while increasing AR improves cruise performance, increasing it too much can be dangerous for wing integrity, and may even increase MTOW, when accounting for the increase of wing mass.
- **Forward propulsion:** As stated before, all the horizontal propulsion is provided by one single ICE engine. A more powerful engine will no doubt be able to meet all the horizontal flight constraints, however, it will also be heavier, more expensive and complex than a less powerful engine. Thus, keeping in mind that low complexity is an important design goal, we prioritized low power yet efficient engines over heavier more powerful engines.
- **Mean chord:** This issue will be further explored on the wing design section of this paper, however, the mean chord has some implications on the aircraft as a whole: for our

current configuration, with the back rotors mounted behind the wing's, it is important to keep the mean chord down, to give more room between the wing's trailing edge and the rotors.

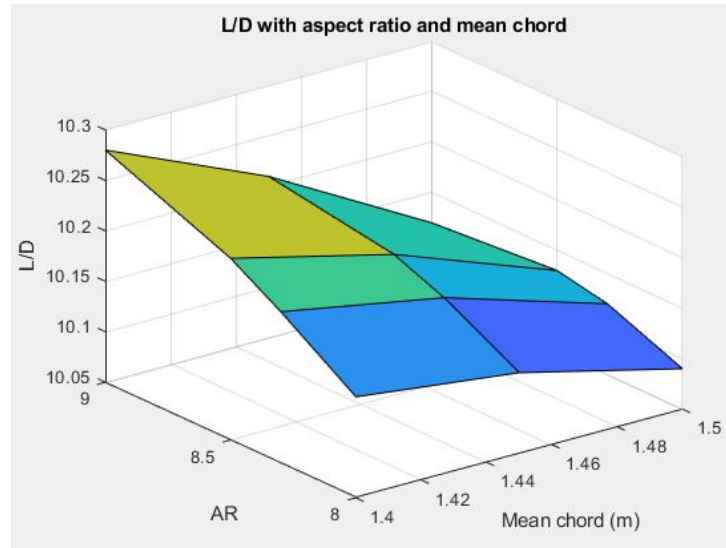


Figure 11: Lift to Drag ratio with Aspect ratio and mean chord

Figure 11 depicts the relation between the wing's properties and the aircraft's Lift to Drag ratio. As written above, an higher Aspect ratio gives a better L/D, and, for a constant AR, decreasing the wing's surface area also increases cruise performance, since it also decreases induced drag.

Nonetheless, Figure 11 also shows very modest increases in L/D for a comparably large increase in AR: the Lift to Drag ratio only increases from roughly 10.1 to 10.3, when the aspect ratio is increased from 8 to 9. For this reason, it was decided to settle for a compromising AR of 8.5, which gives some of the benefits of a large span, whilst keeping the low mass and loads of a small wing.

3.3 Vertical Flight

- **Rotor Diameter:** Rotor Diameter is deeply tied to disk loading, meaning that it can be easily retrieved just by looking at the vertical constraints. However, the size of each rotor also has implications on the mass of the aircraft, and, above all, on the noise produced by the aircraft, which is one of the major design bottlenecks of this project. Moreover, besides the design space and noise constraints, there are also space constraints imposed on the size of the back rotors: if they are roughly above 1.5 meters, they can touch the trailing edge of the wing or at least disturb the flow around it.
- **Vertical propulsion:** Just as for the choice of forward propulsion, choosing the engines used for vertical propulsion is a compromise between power and complexity: a more powerful set of engines will allow for a quicker landing and take off, however it will increase the plane's mass, specially the battery's.

3.4 Design Point

In this subsection the final design point will be presented and its rationale explained.

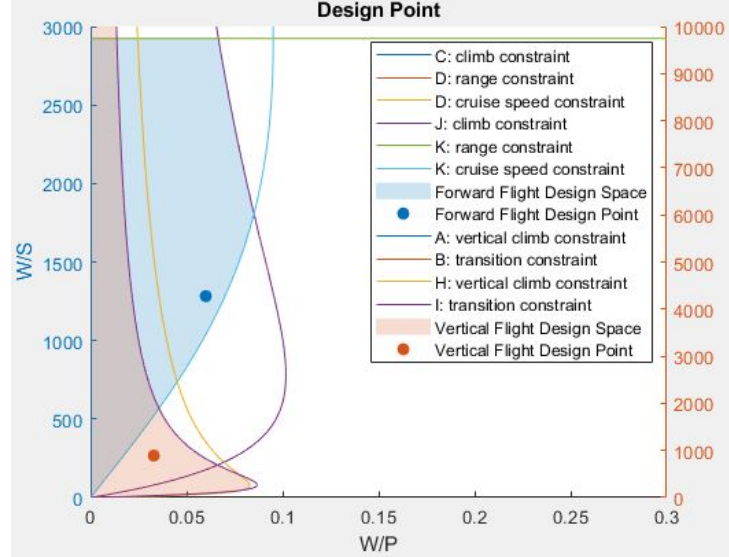


Figure 12: Design point

The final forward design point, in blue, is well inside the mission's design space: as seen in Figure 10, the aircraft is capable of operating at even larger velocities. As for its wing loading, it is also comfortably inside the requirements, so as to enable the aircraft to carry heavier payloads if necessary.

The final vertical design point is likewise well inside the required design space. The details concerning propulsion design will be discussed further on, nevertheless, it is worth mentioning that the noise-at-hover constraint is much more stringent than the design space itself. As for the vertical power loading, whilst it may seem excessive, given how to the left of the constraint the design point is, it is of paramount importance that the aircraft has enough excess vertical power. This makes take offs easier, quicker and safer, and adds flexibility to the design.

4 Wing Design

The wing design objectives are similar to the early aircraft sizing goals presented above:

- Good performance at low Reynolds number ($Re=8e9$), given that the cruise speed is 84 m/s.
- Low stall speed, enabling the aircraft to cruise at even lower speeds and decreasing the horizontal power requirement.
- Low complexity, in order to reduces costs

4.1 Airfoil Selection

Given the requirement of good performance at low speed, it was decided to choose between high camber airfoils, since they have higher maximum lift coefficients, lower stall speeds and are more stable at low speeds. Additionally, it was decided to choose high thickness airfoils, again for their high lift coefficient.

High camber and thickness airfoils tend to have a larger C_d for the same C_l , which translates to a higher induced drag on the 3D wing, however, the aircraft operates at low speeds, which makes the form drag's contribution much larger relatively to the induced's one. 54, a high lift coefficient is needed for the transition segment, when the aircraft's horizontal speed is almost null. Thus, a better transition performance was prioritized over a better cruise performance.

The top two airfoil contenders were the NACA 4412 and the NACA 4418, shown below:

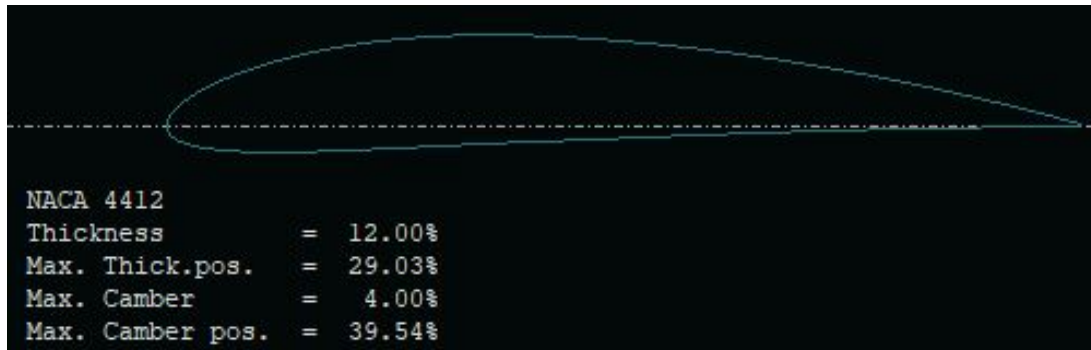


Figure 13: NACA 4412

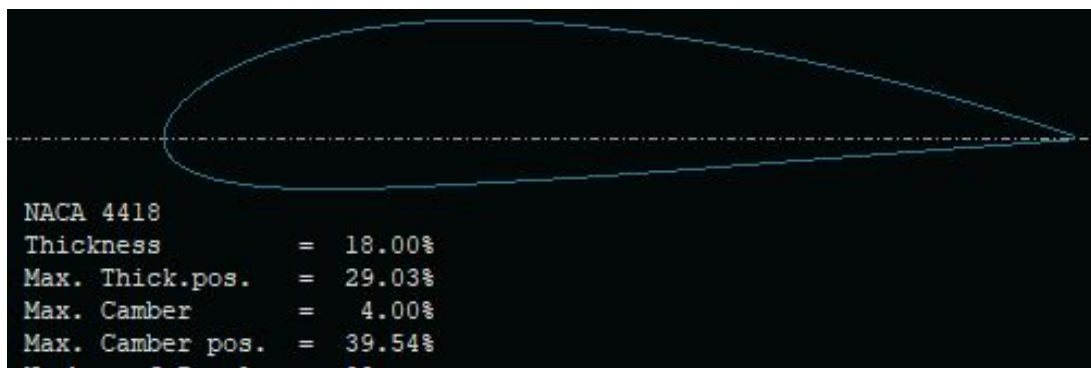


Figure 14: NACA 4418

As mentioned above, high camber wings tend to have better performance at low speeds, due to their higher C_l 's. This is invaluable to this aircraft on the transition and climb segments, as

it can not rely on a typical horizontal take off to increase speed and lift. Both airfoils depicted above have a maximum camber of 4% at roughly 40% of their chords.

Therefore, their only major distinction is their thickness: the NACA 4412 has a 12% thickness at roughly 30% of its chord, while the NACA 4418 has a 18% thickness, at the same x .

The effects of this disparity will be discussed on the next few paragraphs:

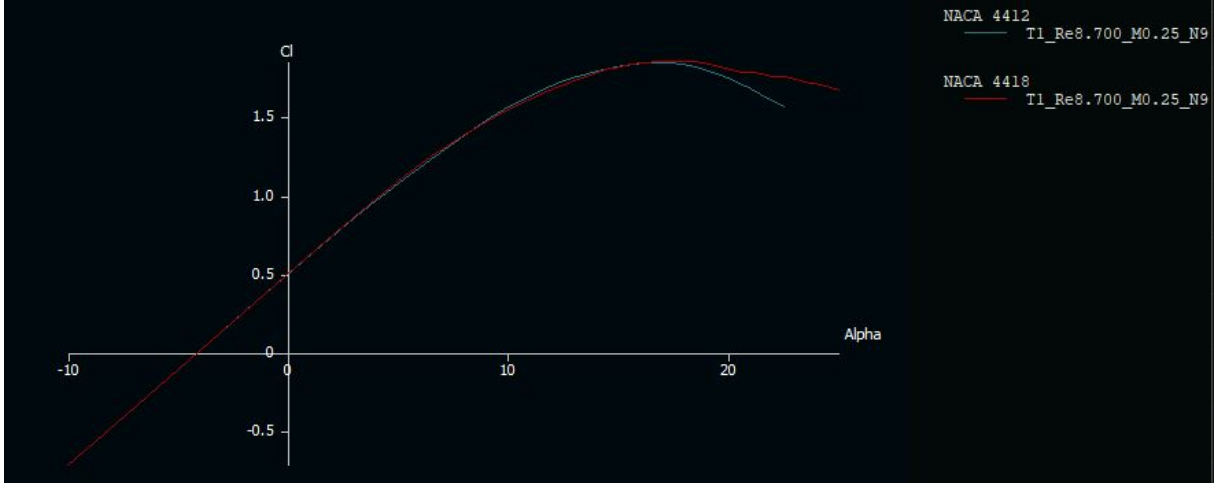


Figure 15: C_l with α for the NACA 4412 and NACA 4418 airfoils

Figure 15 shows that both airfoils have a very similar C_l for each α , specially for low angles of attack. Notwithstanding, the NACA 4418 airfoil does have a slightly higher C_l and $C_{l\alpha}$ and stall angle than the NACA 4412

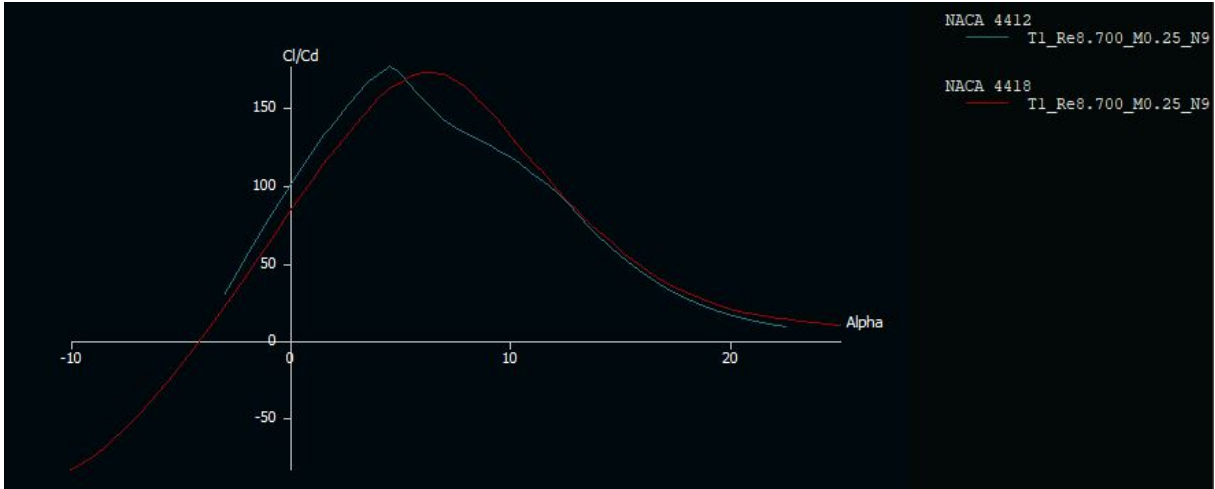


Figure 16: C_l/C_d with α for the NACA 4412 and NACA 4418 airfoils

As for their C_l/C_d , the NACA 4412 has a clear advantage, having a much higher lift to drag ratio than the NACA 4418. This is a clear byproduct of the high thickness of the latter. While the wing's induced drag has a relatively small contribution to the aircraft's total Drag in cruise, it is still important to minimize it whenever possible.

In this case, the NACA 4418 airfoil has a much larger C_d , whilst having a negligible increase in C_l , hence, it was decided to use the NACA 4412 for this aircraft's wing, due to its good performance at low speeds, high C_l , and lower C_d relative to other high camber wings.

4.2 3D Wing Design

With the airfoil selected, all that is needed to finishing designing the wing is selecting its 3D parameters: Aspect ratio, sweep angle and taper ratio. Some of these have intricate and complex relations with other sections of this project, and their values have been iterated many times, so do bear in mind that the rest of the project is as much a product of this wing design as the latter is a product of the rest of the project.

4.2.1 Aspect Ratio

As was mentioned on the previous section, increasing the wing's aspect ratio is often an easy and cost effective way of improving the aerodynamic cruise performance. After the parametric study of the effects of changing AR, an aspect ratio of 8.3 was set, which, for $S = 17.45m^2$ results in a span of 12 m. This value of AR is inside the general aviation recommended range of values, and the span is not too high, resulting in a favorable wing mass and integrity.

4.2.2 Sweep Angle

Given that the aircraft will be subsonic, the only reason for having a swept wing is to increase its lateral stability. On the other hand, a swept wing will be more expensive to manufacture, and will slightly complicate rotor placement. Ergo, it was decided to have a sweep angle of 0, as its main benefit of increased stability can be achieved less expensively by increasing the size of the vertical stabilizer or some its properties.

4.2.3 Taper Ratio

A simple tapered wing has a better aerodynamic performance, namely, it has a lower induced drag coefficient than a rectangular wing, at the cost of having a larger span for the same wing area, and being more expensive to manufacture. On the other hand, whilst having a worse lift distribution, a rectangular wing has a lower stall speed, which is particularly handy in this case, and is significantly less expensive to produce. A rectangular wing was decided for this aircraft, since its benefits: low cost and, particularly, low stall speed, outweigh its main drawback: having a higher induced drag, specially considering the form drag is such a large part of the total drag in cruise, when compared to the induced drag.

4.3 Lift and Drag Estimation

The Lift and Drag in cruise will be presented explained below, for a nominal cruise segment, at 1500 m of altitude and 85 m/s. The fuselage's form Drag coefficient was estimated using the *MATLAB* tool referred previously:

$$(C_{D0})_{fuselage} = 0.0197. \quad (4.1)$$

This is a high Drag coefficient, which can be explained by the fuselage's size when compared to the total aircraft's mass. On the other hand, the wing's form Drag coefficient is much smaller:

$$(C_{D0})_{wing} = 0.0085 \implies (C_{D0}) = 0.0282. \quad (4.2)$$

The aircraft's zero lift coefficient is unsurprisingly high, which does have negative consequences for the cruise efficiency. As for the wing's induced drag, assuming a low angle of attack:

$$C_L = \frac{W}{\frac{1}{2}\rho S_w V_c^2} = 0.3445 \implies C_{Di} = 0.0057. \quad (4.3)$$

One relevant take away from these equations is that the wing's induced Drag provides a very small contribution to the overall Drag. As for the total Drag, and the lift to drag ratio, it can be easily computed using the results above:

$$C_D = C_{D0} + C_{Di} = 0.0339 \implies D = 2201N \implies \frac{L}{D} = 10.17. \quad (4.4)$$

However, if we consider the ratio between the Lift and Drag produced by the wing alone, the Lift to drag ratio is:

$$\left(\frac{L}{D}\right)_{wing} = 24.26. \quad (4.5)$$

It is important to remark that the Drag estimated in this section is produced by the fuselage and wing alone. The form Drag of the propeller, rotors and the bars connecting them to the fuselage were not considered.

The rationale behind the use of 6 blades for each rotor will be explained further on the propulsion design section, notwithstanding, it is relevant to explain why it was not decided to use only 2 blades per rotor: a 2 bladed rotor would have much less drag in forward flight, however, due to the stringent vertical power constraints, the 2 blades would have to be much longer and thicker, meaning that the noise produced by them would be well above the 80 dB at 500 m. Therefore, a 6 blade rotor configuration was decided: it produces much less noise than 2 blades (86 dB to 74 dB), and while it produces much more Drag in forward flight, the propulsion chosen can easily take on this extra Drag. The main idea behind this compromise between noise and forward power is that it is much easier to increase the forward power installed, than it is to decrease the noise emitted by the aircraft in hover.

In conclusion, this aircraft's wing is responsible for roughly 40% of the total Drag. With this final result, the aircraft's Drag in cruise is easily matched by a conventional ICE turboprop + propeller setup, as will be discussed further on.

5 Tail design

The tail assembly of an aircraft, also commonly referred to as empennage, has two main components, the horizontal tail and the vertical tail, which play a major role in balancing and stabilizing the aircraft both longitudinally and directionally, respectively.

The horizontal tail also acts as a lifting surface, as the horizontal tail generates a small lift force crucial for balancing the pitching moments generated by the main wing and fuselage, among others. It also acts as a stabilizer of rotational motion around the y axis of the aircraft.

Likewise, the vertical tail can generate a lateral force that pushes the rear of the aircraft towards an alignment with the airflow, thus stabilizing the vehicle laterally. However, since the aircraft is symmetrical in relation to the xz plane, the vertical tail does not play an important balancing role like its horizontal counterpart.

5.1 Tail Configuration

There is a vast number of tail configurations to choose from, each with its own intricacies, strong points and weaknesses. Choosing a configuration should be the first step in tail design, since it heavily influences the parameters used for sizing each of the stabilizers, which shall be contemplated in section 5.3. The configuration chosen should be the one that best satisfies the design requirements and will probably be a compromise solution.

Many options were considered, such as conventional tails, T-tails, H-tails and canards. The conventional aft tail configuration is a common and all-round acceptable solution that grants a minimum weight to the assembly. On the contrary, T-tails and H-tails usually weigh more than an equivalent conventional tail design. The concept's MTOW value is considerably below the requirement, so the weight was not the most important factor in this decision, even though lowering the weight of the vehicle is a priority of this study. However, since a T-tail provided no clear benefits relative to a conventional tail, it was discarded as an option.

Using canards as horizontal stabilizers was also discarded, since it would be more complex and aerodynamically less sound. Placing lifting and control surfaces in the wake of the forward engine is not desirable, due to a loss in efficiency.

One characteristic of H-tails is that the twin vertical tails act as winglets of the horizontal tail, improving its aerodynamics and allowing it to have a smaller span. This could be useful in the design, since there isn't much space available in the fuselage to place the empennage due to the presence of the aft cabin door and the fuselage being already as long as the requirements allow it to be.

An H-tail configuration also provides higher manoeuvrability and having two vertical stabilizers far from the centerline of the aircraft guarantees they are not affected by the wake of the propeller. On the other hand, because the horizontal stabilizer also becomes smaller, it stays further away from the turbulence generated by the inactive rotors during horizontal flight.

Moreover, during the concept phase, an H-tail that connects to the wings using tail booms, where the electric motors for VTOL would be attached, was considered. For that reason, maintaining an H-tail configuration allows for an easier conversion of the design to that idea, if needed.

Concluding, and having reviewed all the appropriate and feasible configurations, the H-tail option seemed more suitable than a conventional tail for this design.

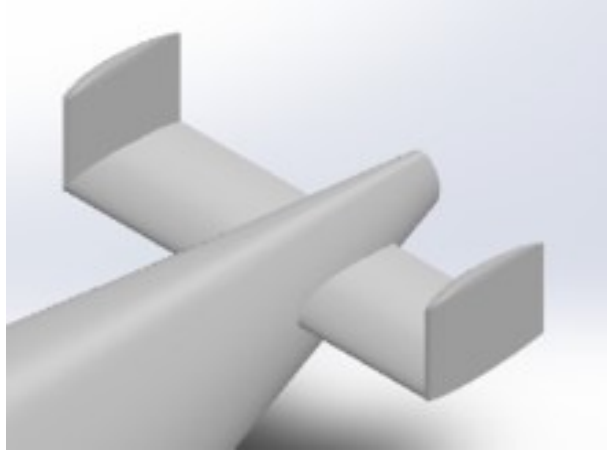


Figure 17: H-tail configuration as viewed on the concept CAD.

5.2 Airfoil selection

The horizontal and vertical stabilizers are, after all, wings, and like with any wing design, an airfoil must be chosen. Since generating lift is not really a requirement, the focus should be on minimizing drag. In fact, the tail should only produce lift when the control surfaces are actuated, generating an artificial camber to the airfoil. Thus, a symmetric airfoil, with a low base drag coefficient, C_{D_0} , is the obvious choice.

Having high control authority at low speeds and a high $C_{L\alpha}$ was also a design objective. The H-tail configuration already grants a "boost" to the C_L derivative with α , but choosing an airfoil with a high base $C_{l\alpha}$ value is key.

After searching for low-speed symmetric airfoils, the 4-digit NACA series of airfoils appears to be appropriate and both NACA 0012 and NACA 0010 were under appreciation. It's generally a good practice to have the local Mach number on the tail lower than that of the main wing. One way to guarantee that is to have the tail airfoils be thinner, making the NACA 0010 the chosen airfoil for both the vertical and horizontal stabilizers. This airfoil has a 10% thickness at 30% of the chord.

5.3 Sizing

Having established a wing design, as detailed in section 4, the tail can be sized by resorting some geometric relations, using wing parameters as inputs and interpolating from historical data.

Two of those parameters are the tail coefficients, c_{VT} and c_{HT} , which were derived mainly from statistical data for the first design iteration. According to [9], for General Aviation (single engine) aircraft, the base vertical tail coefficient, c_{VT} , should be 0.04 whereas c_{HT} is 0.70. However, due to the irregular shape of the aircraft, given by its VTOL components, some adaptation was needed to ensure directional stability. Namely, it was decided to double the value of c_{VT} , similar to what a twin turboprop aircraft would need, to balance the effect of having 4 rotors on the side of the vehicle.

Then, these tail coefficients should be scaled according to the H-tail configuration chosen. As stated before, the H-tail divides the vertical tail into two twin surfaces, so to obtain the area of each one, the equivalent vertical tail coefficient becomes $c_{VT_{eq}} = 0.5 c_{VT} = 0.04$. [9]

Moreover, because the horizontal tail is between the verticals, its efficiency is increased so a scaling factor of 95% can be introduced, reducing its size. That is, $c_{HT_{eq}} = 0.95 c_{HT} = 0.665$.

Finally, the size, or area, of the horizontal and vertical stabilizers is given, respectively, by the following equations, from [9]:

$$S_{HT} = c_{HT_{eq}} \frac{\bar{c}_w S_w}{l_{HT}} \quad (5.1)$$

$$S_{VT} = c_{VT_{eq}} \frac{b_w S_w}{l_{VT}} \quad (5.2)$$

where $l_{HT} = l_{VT}$ is the distance between the aerodynamic centers of the main wing and the tail. As an approximation, the aerodynamic centers are considered to be at the center of mass of the lifting surfaces. Again, looking at typical lengths for other aircraft, a relation of $\frac{l_{tail}}{l_{fuselage}} \approx 0.5$ can be observed [9], where l_{tail} can mean either l_{VT} or l_{HT} . Then, using $l_{fuselage} = 10 m$, the distance between the aerodynamic centers comes as

$$l_{tail} = \frac{l_{tail}}{l_{fuselage}} \times l_{fuselage} = 0.5 \times 10 = 5 m$$

This first approximation was kept throughout the design, as can be confirmed when looking at the position of the wing and tail sections of the aircraft, on Table 6, and checking the difference between them is five meters.

In conclusion, using the geometric parameters discussed above, the main wing characteristics from section 4 and equations (5.1) and (5.2), it is possible to compute the area of the stabilizers as follows:

$$S_{HT} = 0.665 \times \frac{1.45 \times 17.45}{5} = 3.37 m^2$$

$$S_{VT} = 0.04 \times \frac{12 \times 17.45}{5} = 1.68 m^2$$

where S_{VT} is half of the total vertical surface area, that is, it corresponds to one side of the tail only. The rest of the tail parameters originate from two further definitions:

- the span b of the horizontal stabilizer is fixed and equal to 3 meters;
- the chord length \bar{c} of the vertical and horizontal tails should be the same.

The first definition ensures that a significant part of the horizontal stabilizer - and the attached vertical stabilizers - are outside of the wake of the propeller engine, but still not far enough to be under the disturbed airflow coming from the inactive rotors. On the other hand, the second assumption is for simplification purposes only, both of design and construction.

From here, the aspect ratio and other remaining parameters can be deduced and are presented on Table 2 below.

Table 2: Tail geometric parameters.

	Horizontal Tail	Vertical Tail (each)
Surface Area, S	$3.37 m^2$	$1.68 m^2$
Aspect Ratio	2.67	1.34
Span, b	3 m	1.5 m
Mean chord, \bar{c}	1.12 m	1.12 m

6 Fuselage

In this section, the design of the external and internal layouts of the fuselage is studied. The purpose of this vehicle is to perform three different types of mission, naturally resulting in different internal layouts that should be easily interchangeable.

6.1 Internal Dimensions

As stated in the mission requirements, the vehicle should be able to operate as air taxi, aeromedical and cargo. Since the internal arrangement and components of the payload are different for each type, the aircraft is equipped with a rail system that enables the removal of seats through the main door, located in the aft fuselage.

6.1.1 Standard Air Taxi

When operating as Air Taxi, it is expected to carry four passengers plus one pilot and 100 kg of luggage, corresponding to a total payload of 600 kg. The top view of the configuration is presented in Figure 18.

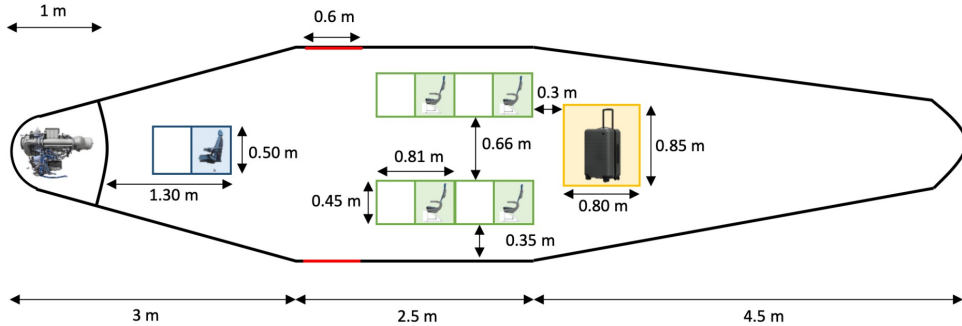


Figure 18: Air Taxi configuration.

The dimensions and spacing of the seats were determined according to Table 3, from [9].

Table 3: Passengers' seats and aisle dimensions

	Short range	Chosen
Seat width (in)	16-18	18
Seat pitch (in)	30-32	32
Aisle width (in)	>15	22
Aisle height (in)	>60	72

Since the number of passengers is small, the maximum dimensions of seat width and pitch were chosen in order to provide a more pleasant experience, with two rows in 1+1 arrangement.

The aisle height selected is 72 in (1.82 m) so it allows a person with average height to be standing comfortably and the paramedic to work beside the stretcher in the aeromedical configuration.

Considering the already determined dimensions, a diameter of 2.25 m is selected, allowing for a underfloor compartment of 43 cm, that will store components such as batteries and avionics, as discussed in further sections.

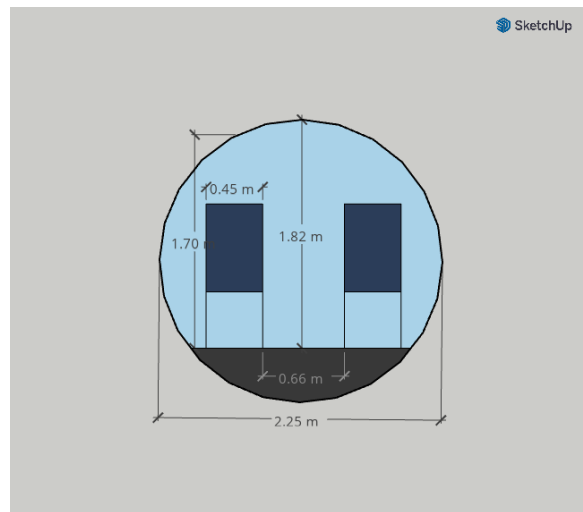


Figure 19: Cross section of the cabin

6.1.2 Aeromedical

In this mode of operation, the fuselage should accommodate one stretcher, one patient, one paramedic and 100 kg of equipment as well as the pilot, as shown in Figure 20. All the seats except one for the paramedic are removed using the aforementioned system.

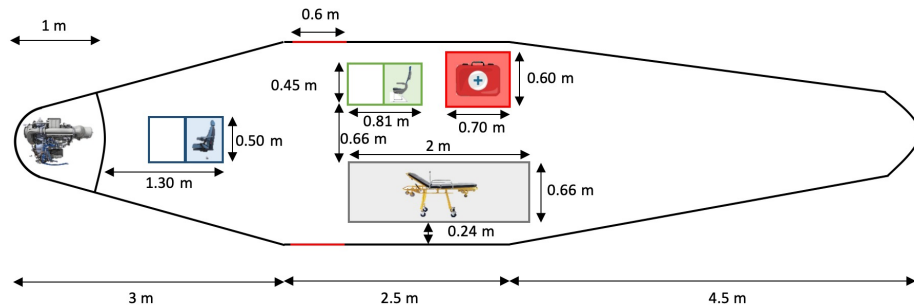


Figure 20: Air ambulance configuration.

6.1.3 Cargo

Finally, in Cargo mode, the aircraft must have the dimensions to fit a standard forklift pallet (40 in x 40 in x 48 in, or, 1 m x 1 m x 1.2 m) of 500 kg. Since all the seats can be removed, it is confirmed that there is enough space for the payload when considering the previously chosen dimensions, as in Figure 21.

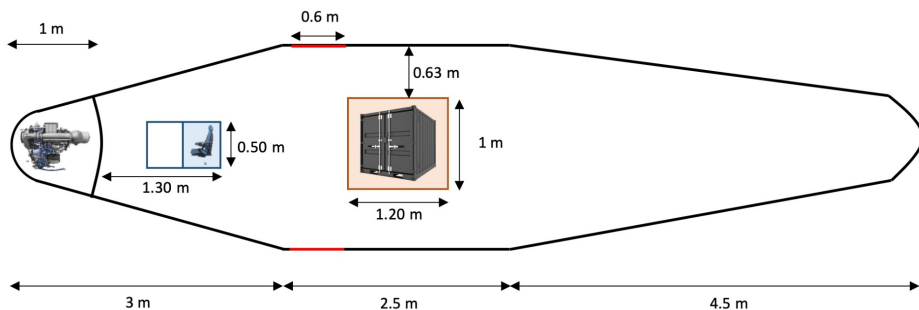


Figure 21: Cargo configuration.

6.2 External Dimensions

The length and diameter of fuselage as well as its shape are estimated taking into account historical values and aerodynamic considerations.

It is possible to determine the length using the table from Figure 22, for a single engine aircraft, which yields a length $l_f = 9.47$ m, for the most recent MTOW of 2282 kg. Since this is an iterative process, the length calculated for the earlier MTOW was approximately 10 m, so it was decided to keep this value as it better satisfies the stability margins and space constraints for the rotors.

$\text{Length} = a W_0^C$	a	C
Sailplane—unpowered	0.86	0.48
Sailplane—powered	0.71	0.48
Homebuilt—metal/wood	3.68	0.23
Homebuilt—composite	3.50	0.23
General aviation—single engine	4.37	0.23
General aviation—twin engine	0.86	0.42
Agricultural aircraft	4.04	0.23
Twin turboprop	0.37	0.51
Flying boat	1.05	0.40
Jet trainer	0.79	0.41
Jet fighter	0.93	0.39
Military cargo/bomber	0.23	0.50
Jet transport	0.67	0.43

Figure 22: Fuselage length vs W_0 (imperial units) [10]

The diameter was already determined by the passenger requirements, thus the fineness ratio, defined as $\frac{d}{l}$, can be calculated. The value obtained is 0.225, which is located near the bottom of the C_{D0} vs $\frac{d}{l}$ plot in Figure 23, thus minimizing the contribution of the fuselage to the drag.

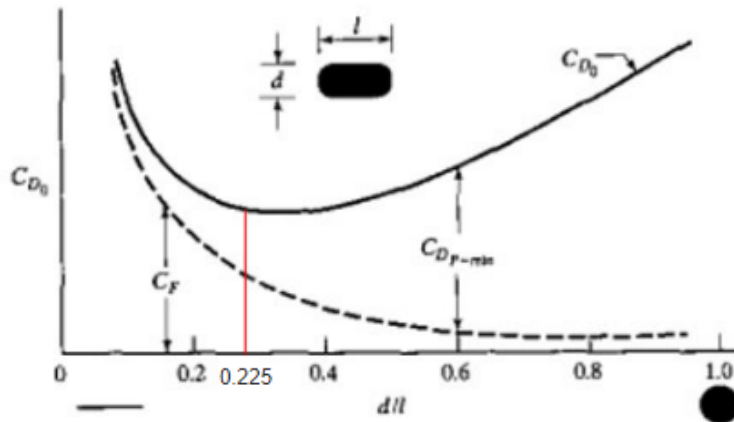


Figure 23: Fineness ratio in subsonic vs C_{D0}

It was also a requirement that the aircraft must provide an easy access for reduced mobility passengers and an external door that enables the use of a forklift to load the aircraft. The solution presented is a rear cargo-like door, which deploys from the bottom of the upswept portion of the aft fuselage and serves as a loading ramp for passengers and cargo when lowered.

Regarding the rear part of the fuselage, Figure 24 gives some guidelines on typical values. A $\frac{l_t}{d} = 2$ was chosen, yielding a length of the rear fuselage cone of 4.5 m. The divergence angle

should not be higher than 25° [10], and the decision of using 18° was made, so that the height from the bottom line to the upper fuselage is approximately 1.5 m. Naturally, this height needs to be higher in order to be comfortable for the passengers to enter/exit and to allow for the use of a forklift, but one must not forget the increment in height that will be given by the landing gear (subsection 6.3).

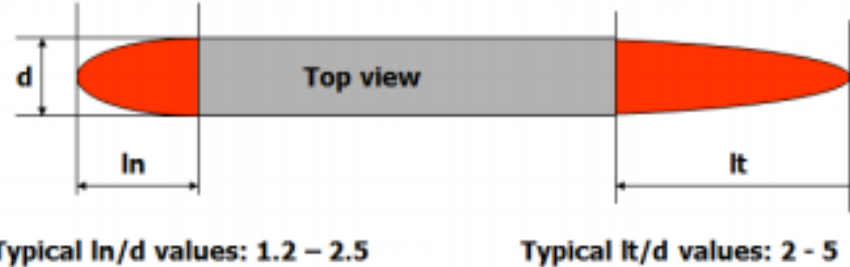


Figure 24: Fuselage length ratios [11]

Finally, the nose length was chosen to be 3m, so that there is enough space to fit the front propeller engine and the cockpit. The length of the central part yields $10 - 4.5 - 3 = 2.5$ m, which is perfectly admissible considering the dimensions of the elements in the configurations previously defined.

6.3 Landing Gear

Although the aircraft is supposed to perform vertical take-off and landing, there is a requirement stating that it should have the capability to be easily moved in the ground. For that reason, the landing gear will take a tricycle configuration with wheels, instead of the traditional skids that other VTOL aircraft present. The option of using the former but landing on a moving cart was thought off but quickly discarded, since it is not a safe operation for a commuter aircraft, despite all the advantages it might bring. The decision to follow was that of using a fixed landing gear, as it is cheaper, lighter, easier to manufacture and maintain, and also provides more stability. The consequence of such configuration is the increased drag, so the incorporation of fairings on the wheels was embraced, since it may reduce up to 1000% of the wheel drag. [12]

A brief study of the wheel size was performed, using the equation and values for the General Aviation category in Figure 25, and a diameter and width of approximately 19 in x 7 in was obtained. These values are coherent when comparing to similar aircraft such as the Cessna 172 (17 in x 6 in). [13]

Main wheels diameter or width (in.) = $A \cdot W_W^B$				
	Diameter		Width	
	A	B	A	B
General aviation	1.51	0.349	0.7150	0.312
Business twin	2.69	0.251	1.170	0.216
Transport/bomber	1.63	0.315	0.1043	0.480
Jet fighter/trainer	1.59	0.302	0.0980	0.467

W_W = Weight on Wheel

Figure 25: Wheel sizing [10]

Finally, the height of the landing gear was chosen to be 1 m, so it provides a safe amount of ground clearance for both the propeller and the rotors, that are connected to the bottom of the fuselage, and for the access ramp to deploy as mentioned before.

6.4 Other Structural Components

The selected concept (Figure 8d) presents two identical booms mounted on the wing to support the vertical rotors. However, this configuration would result in a significant increase in the wing's weight, that would need stronger spars and ribs to support the stress caused by the rotors. The booms would also cause discontinuity in the leading edge, compromising the forward flight performance.

Therefore, the solution proposed consists in mounting the booms transversely through the bottom of the fuselage, which would not cause flow interference in the wing, and is a much easier and cheaper configuration. The main drawback is the increase of drag, whose quantification requires a more complex fluid dynamics analysis and is out of the scope of this conceptual approach. The two booms are identical, placed symmetrically with respect to the center of gravity, with a circular cross-section of 30 cm of diameter and 7 m of length, which allows for the rotors to rotate at a safe distance from the fuselage. These dimensions were used to compute the maximum deflection of a cantilever beam with an end load corresponding to the thrust generated by the rotors, and for a large range of materials (Young's Modulus), the deflection was negligible and below the maximum allowable deflection of beams. [14]

7 Structural Design

7.1 Flight Envelope

In this subsection, the expected loads that the aircraft can safely experience will be estimated through a V-n diagram with and without gust loads. The group also developed a MATLAB script to compute and plot this diagram, in order to be able to iterate with more ease and perform parametric studies. The steps followed for the implementation are discussed below.

Recalling that the cruise speed considered is 84 m/s, the dive condition $V_{dive} = 1.5V_{cruise} = 126$ m/s is assumed. The load factors are obtained from FAR-25 [15] and FAR-23 [16]:

$$\begin{cases} n_{max} = 2.1 + \frac{24,000}{MTOW + 10,000} = 3.7 \\ n_{min} = -0.4 \cdot n_{max} = -1.48 \end{cases} \quad (7.1)$$

With these load factors, the velocities for the positive and negative high angle of attack condition, $V_A = 70$ m/s and $V_B = 44$ m/s respectively, can be determined from:

$$n = \pm \frac{0.5\rho V^2 C_{Lmax}}{W/S} \quad (7.2)$$

by substituting n_{max} and n_{min} , where ρ is the air density at 1500 m and W/S is the wing loading from the design point.

In order to account for gusts, the following factors are calculated:

$$\mu = \frac{2W/S}{\rho g \bar{C} C_{L\alpha}} = 37.92 \implies K = \frac{0.88\mu}{5.3 + \mu} = 0.772. \quad (7.3)$$

The cruise altitude is 1500 m, so the statistical values for the gust velocity below 20,000 ft present in Figure 26 are used.

TABLE 10.3: Statistical gust velocity values.

Flight Condition	Altitude Range (ft)	\hat{u} (ft/s)
High Angle of Attack	0–20,000	66
Level Flight	0–20,000	50
Dive Condition	0–20,000	25
High Angle of Attack	50,000	38
Level Flight	50,000	25
Dive Condition	50,000	12.5

Figure 26: Statistical gust velocities [9]

Finally, the increase in the load factor for level flight ($n = 1$) is given by:

$$\Delta n = \frac{0.5\rho V C_{L\alpha}}{W/S} \cdot K \hat{u}. \quad (7.4)$$

The combined V-n diagram is shown in Figure 27. As seen, the limit loads are mostly determined by the basic V-n diagram, concluding that the loads induced by gusts do not have a significant impact on the structure.

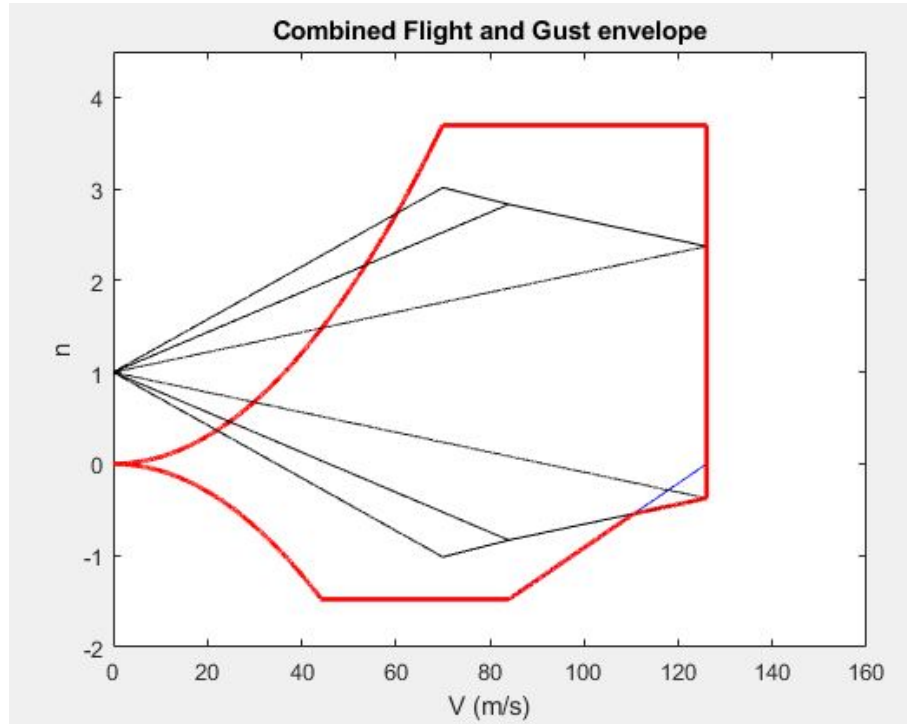


Figure 27: Combined V-n diagram

7.2 Shear stress and bending moment

7.2.1 Wing

To properly design the structure of the wing it is first necessary to determine the loads subjected to it. Since neither the engines or the rotors are mounted in or under the wings, the only loads analyzed are the lift produced by the wings the weight of the structure itself. So, the first step is to estimate these loads.

For estimating the weight, equation (7.5) [9] was used.

$$W_{wing} = C_1 C_2 C_3 W_{dg}^{C_4} n^{C_5} S_w^{C_6} \mathcal{R}^{C_7} (t/c)^{C_8} (C_9 + \lambda)^{C_{10}} (\cos \Lambda)^{C_{11}} S_f^{C_{12}} q^{C_{13}} W_{fw}^{C_{14}} \quad (7.5)$$

In the equation above:

- W_{dg} is the design gross weight (lbs)
- n is the design load factor
- S_w is the wing area (f^2)
- \mathcal{R} is the aspect ratio of the wing
- (t/c) is the maximum thickness-to-chord ratio of the wing
- λ is the taper ratio
- Λ is the sweep angle of the maximum thickness line ($^\circ$)
- S_f is the area of the flapped portion of the wing
- q is the dynamic pressure at cruise conditions (lbs/ f^2)
- W_{fw} is the weight of fuel stored in the wings

- the coefficients C_i can be consulted in Table 11.1 of Corkes's Design of Aircraft [9], and correspond to the general aviation category.

It was considered a design load factor of 4.4, a typical value for this type of aircraft [9]. All other values are mentioned in the previous sections of this report. According to this data, the estimated wing weight is $W_{wing} = 2116N$. This weight was considered to be uniformly distributed along the wingspan.

When it comes to lift estimation, the trapezoidal approximation was used. In the case of our untapered wing, the lift distribution is simplified in a uniform distribution along the wingspan. Therefore, the distribution of forces applied in half a wingspan (taking into account that the wing is symmetric) is as represented in Figure 28.

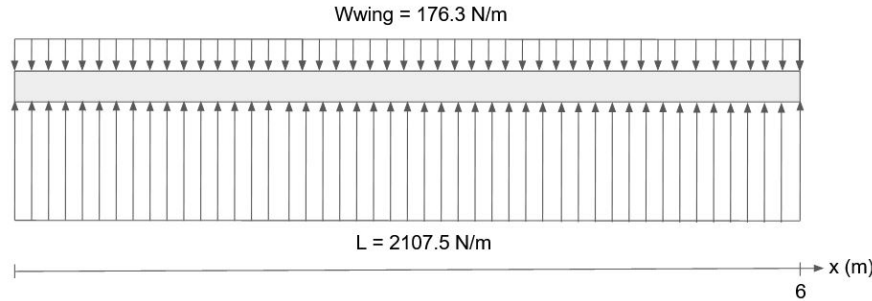


Figure 28: Distribution of loads across the wing

The shear force and bending moment diagrams for the wing are shown below. In these figures, due to the symmetry of the wing, only half the wingspan was considered.

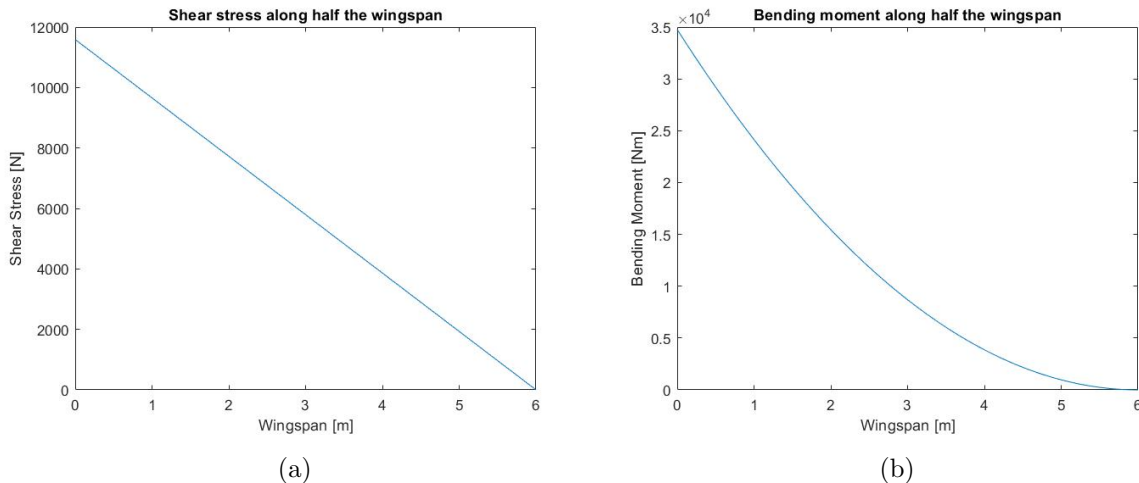


Figure 29: Shear stress (a) and bending moment (b) along half the wingspan.

Since the wing is supported at the root by the fuselage, the applied loads result in increasing shear and bending moments towards the wing root. The critical (maximum) values are summarized in Table 4.

Table 4: Maximum values for shear force and bending moment in the wing.

Shear force	11590 N
Bending moment	34760 Nm

7.2.2 Fuselage

The study of the load distribution along the fuselage allows the determination of the maximum loads that the fuselage is subjected to. These parameters are extremely important for fuselage design and material selection.

In order to determine the load distribution throughout the fuselage, a number of simplifications were made. First, the fuselage was modeled as a beam supported at the location of the center of lift of the wing. Second, all loads were modeled as point loads, except for the fuselage weight, which was modeled as a uniformly distributed load along the fuselage length.

The loads on the fuselage structure were calculated for the three possible aircraft configurations: air taxi, air ambulance and cargo. The weight of the components specific to these configurations can be found in Table 5, and their position along the fuselage is explicit in Figures 18, 20, and 21, for each configuration respectively.

Table 5: Configuration specific aircraft components.

Component	Weight (kg)
Cargo (cargo mode)	500
Passenger and chair	115
Pilot and chair	115
Cargo (Air Taxi mode)	100
Paramedic and chair	115
Stretcher and patient	145
Cargo (air ambulance mode)	300

In addition, the weights and positions along the fuselage length of the components that are present in all configurations can be found in Table 6.

Table 6: General aircraft components.

Component	Weight (kg)	Position (m)
Propeller	10	0
Gearbox	5	0.25
ICE	104	0.50
Avionics	65	1.50
Electric motors/rotors (front)	104	2.00
Landing gear	60	3.00
Fuel tank	25.1	4.00
Main Wing	215	4.80
Electric motors/rotors (back)	104	6.00
Batteries	152.2	5.81
Stabilizer	100	9.80

Since the maximum sheer stress and bending moment in the fuselage occur during forward flight, since the lift is concentrated in one place (wings) instead of spread over multiple points (rotors), the diagrams were calculated for this condition.

The shear force and bending moment diagrams for the three aircraft configurations are shown below.

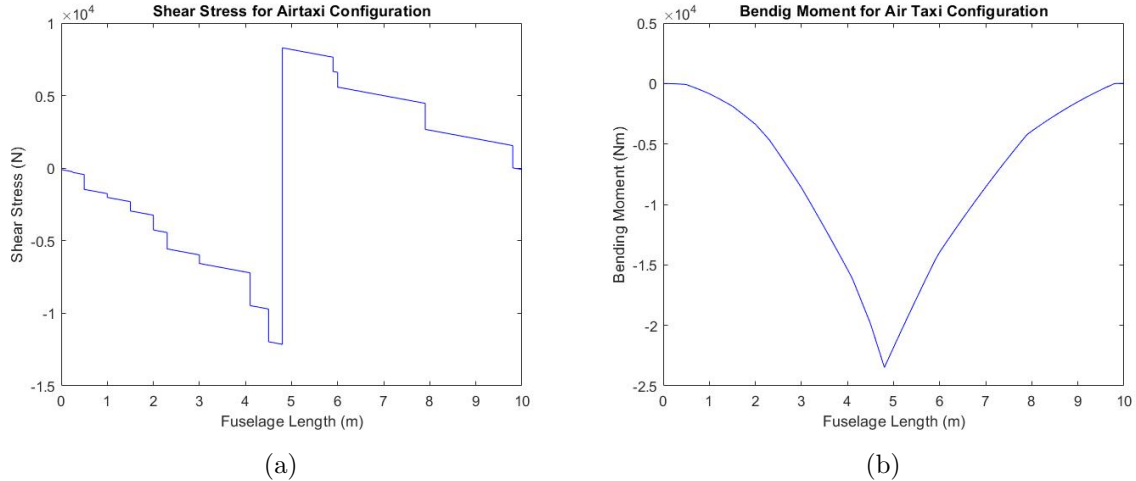


Figure 30: Shear stress (a) and bending moment (b) along the fuselage for the air taxi configuration.

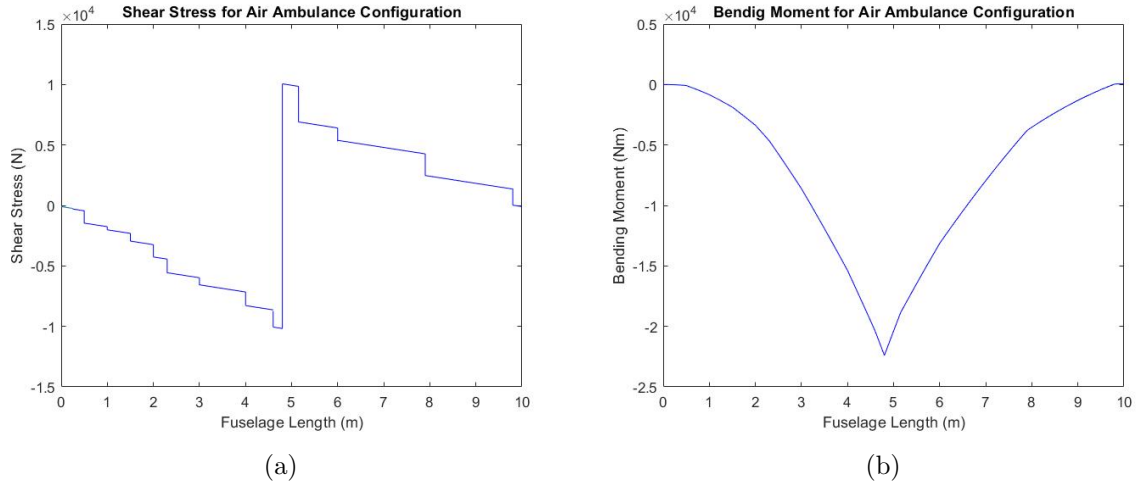


Figure 31: Shear stress (a) and bending moment (b) along the fuselage for the air ambulance configuration.

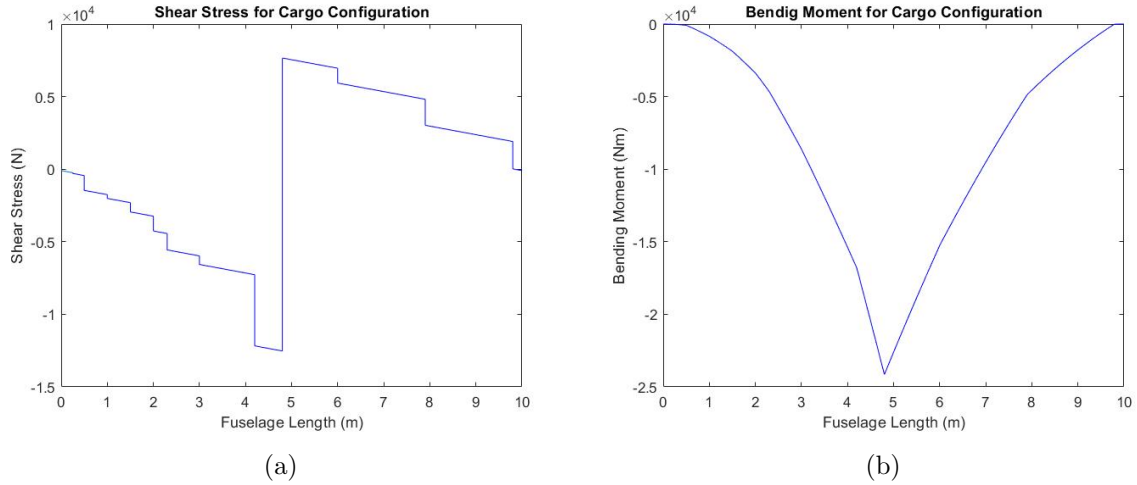


Figure 32: Shear stress (a) and bending moment (b) along the fuselage for the cargo configuration.

Since the maximum absolute values of these two quantities hold a great importance, they are summarized in Table 7.

Table 7: Maximum absolute values for shear force and bending moment in the fuselage.

Configuration	Shear Stress (N)	Bending Moment (Nm)
Air taxi	12140	23480
Air ambulance	12530	24150
Cargo	10050	22400

As we can see from the table, both the maximum shear stress and maximum bending moment along the fuselage are the same for all configurations. However, the highest value for both quantities happens for the cargo configuration. These are the values that need to be taken into account when designing the fuselage structure and during material selection.

7.3 Material Selection

The material selection performed for this aircraft so far has been qualitative rather than quantitative: each aircraft component has been associated with a material, or, in some cases, a mix of them, depending on the operational demands of each component, the characteristics of each material, and their cost.

Furthermore, care was taken to stick to the modern aeronautic trend of using a mix of metal and composite materials, in an effort to reduce the aircraft's empty weight. The following list provides an extensive description of each considered material's pros, cons and uses:

- **Aluminum Alloys:** No modern aircraft design would be worthy of that name without using aluminum: it is safe, easily machined and has excellent mechanical properties, such as a high strength to density ratio and high thermal and electrical conductivity. Its only cons are its higher weight when compared to composites, and its lower strength and elastic modulus when compared to steel. For these reasons, aluminum is a great material for parts of the fuselage, and the airframe.
- **Steel Alloys:** Steel is a very situational material: its strength, resistance, malleability, ductility and durability are arguably unparalleled for its low cost, however, its very high density relegates it to only a small range of applications: usually areas subject to high stress or heat, such as the landing gear or exterior struts.
- **Titanium Steel:** Titanium steel is 45% lighter than regular steel alloys, while still having a very high strength. Its major drawback is its very high cost when compared to other metal alloys, which limits titanium steel to very specific uses, mainly areas subject to very high stress or heat.
- **Carbon fiber:** By far the most used and renowned composite material, carbon fiber has a very high strength to weight ratio, meaning it is very light and rigid. Moreover, it has a negative thermal expansion coefficient, so it does not expand or shrink nearly as much as fiberglass when subjected to temperature changes. Its main drawback is its high cost when compared to aluminum. For all these reasons, carbon fiber is a perfect material for some sections of the fuselage.
- **Fiberglass:** All too often disregarded as a worse version of carbon fiber, fiberglass is much more flexible, cost effective and durable than its more renowned cousin. It does have a lower strength to weight ratio than carbon fiber, however, its flexibility and low cost make it a perfect material for flight control surfaces.

8 Static Stability

The static stability metrics are useful quantities to measure the capability of an aircraft to return to its initial position after a disturbance. In the case of a transport aircraft such as the one this work is trying to design, a stable aircraft is needed. However, the more stable the aircraft, the harder it is to maneuver and so, it is important to keep the stability within certain boundaries.

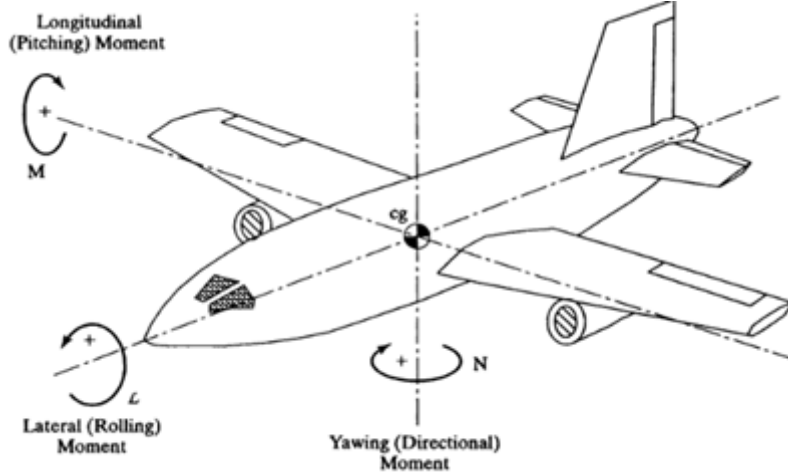


Figure 33: Illustration showing the aircraft axes and directions [9]

In Figure 33, the directions of the moments are illustrated to ease the understanding of equations used in this section.

8.1 Longitudinal stability

The evaluation the longitudinal stability is done in the xOz axis of the aircraft and is directly related to the pitch stability. To evaluate the longitudinal stability of an aircraft, two quantities need to be calculated: the static margin (SM) and the derivative of the pitch moment in respect to the angle of attack ($C_{M\alpha}$) commonly known as longitudinal stability coefficient. The static margin is the distance between the neutral point of the aircraft, in which changing the angle of attack does not change in the pitch moment around that point, and the center of gravity. For the aircraft to be stable, the static margin needs to be positive. That translates to the center of gravity being in front of the neutral point. The longitudinal stability coefficient needs to be negative, so that an increase in angle of attack causes a natural response on the aircraft to decrease its pitch back to the trim condition.

$$SM = \frac{x_{np} - x_{cg}}{\bar{c}} \quad (8.1)$$

The Figure 34 illustrates the distances and forces between the relevant parts regarding the study of the longitudinal stability. As such, the pitch moment coefficient around the center of gravity can be written as:

$$C_{M_{cg}} = \left(C_L \frac{x_w}{\bar{c}} + C_D \frac{z}{\bar{c}} + C_{M_{ac}} \right)_W + \frac{T z_T}{q_\infty S_W \bar{c}} - C_{L_{HT}} \frac{l_{HT} S_{HT} \eta_{HT}}{S_W \bar{c}} - \left(C_{M_{cg}} \right)_I. \quad (8.2)$$

With,

$$\eta_{HT} = \frac{q_{\infty HT}}{q_\infty} \leq 1. \quad (8.3)$$

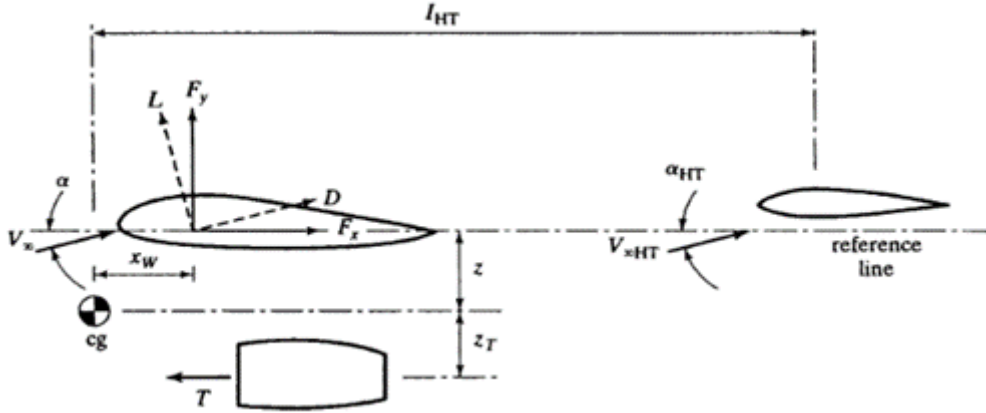


Figure 34: Illustration showing forces and distances on a conventional aircraft [17]

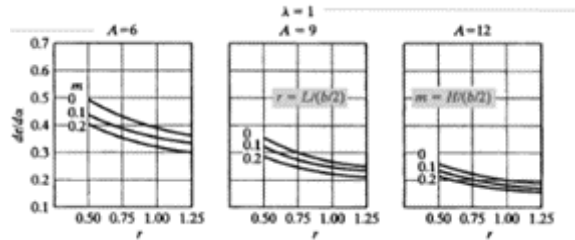


Figure 35: Variation of the downwash factor [17]

The quantity η_{HT} measures the “tail efficiency”, a quantity influenced by the upstream component of the wing velocity caused by the main wing. For this aircraft, $\eta_{HT} = 0.95$ was chosen. The quantity $(C_{M_{cg}})_I$ is the engine term and only applies to turbofan engines. Since the designed aircraft uses a turboprop, this term will be ignored. Lastly, the 3D lift coefficient $C_{L_{HT}}$ for the horizontal tail is given by:

$$C_{L_{HT}} = \frac{\partial C_{L_{HT}}}{\partial \alpha} \left[\left(1 - \frac{de}{d\alpha} \right) \alpha - \alpha_{0L} \right] = C_{L\alpha_{HT}} \left[\left(1 - \frac{de}{d\alpha} \right) \alpha - \alpha_{0L} \right]. \quad (8.4)$$

To get to the stability coefficient the aircraft was considered to be inside the drag bucket and so $C_{D\alpha} = 0$. As a result,

$$C_{(M_{CG\alpha})} = C_{(L_{\alpha_w})} \frac{x_w}{\bar{c}} - C_{L\alpha_{HT}} \left(1 - \frac{de}{d\alpha} \right) \frac{l_{HT} S_{HT} \eta_{HT}}{S_w \bar{c}}. \quad (8.5)$$

The parameter $\frac{de}{d\alpha}$, the downwash factor, was taken from Figure 35 using $H = 0$ and $L = l_h$ and an aspect ratio of 9. As a result, the value used is $\frac{de}{d\alpha} = 0.25$

For the lift coefficient derivatives, the formula from [18] to approximate the 3D lift coefficient derivatives based on the known 2D derivatives (C_{l_α}) for NACA profiles was used.

$$C_{L_\alpha} = \frac{C_{l_\alpha}}{1 + \frac{C_{l_\alpha}}{\pi AR}} \quad (8.6)$$

8.1.1 Procedure

To calculate the static margin and the stability coefficient, the neutral point was calculated using equation (8.5) and equaling it to zero (assume the center of gravity on top of the neutral point for this purpose), so that the derivative of the moment around the neutral point in regard

to the pitch would be null. This approach led to the following value for the neutral point's position:

$$x_{np} = 4.22m.$$

The choice for the center of mass of the airplane was easier and allowed for a certain flexibility in choosing its position due to the nature of mobile batteries. The position of the batteries was calculated after this section in order to place the center of mass in the desired position. As a result, there was the possibility of picking the static margin of the aircraft, which was set to 10%, a value that gives a margin of error big enough for fuel differences during flight and still provide a stable aircraft. For the value of $SM = 10\%$, using equation (8.1), the desired position for the center of mass is as follows:

$$x_{cg} = 4.07m.$$

Lastly, the stability coefficient was calculated using these values, and the result obtained proved that the static stability for this aircraft was assured without making it too stable and unable to maneuver:

$$C_{(MCG_\alpha)} = -1.02 /rad.$$

This value is within the boundaries for stability taught in the theoretical course of:

$$C_{(MCG_\alpha)} \in [-1.5; -0.16].$$

With the centre of gravity determined, the component's lateral arrangement was decided on as follows:

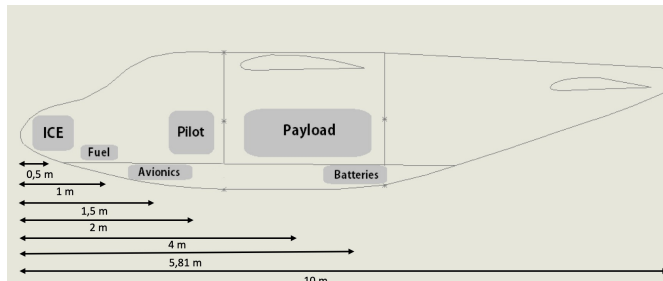


Figure 36: Lateral aircraft arrangement

8.2 Lateral Stability

The rolling moment, represented by L , comprises the focus of the lateral stability. It possesses a positive value when the right wing tip moves down (and the left wing tip moves up). The rolling moment's dimensionless coefficient is represented in equation (8.7).

$$C_L = \frac{L}{qS_W b} \quad (8.7)$$

The lateral stability of an aircraft can be measured by its ability to respond to a gust at an angle of sideslip (yaw) β and can be evaluated through the derivative present in equation (8.8). In the mentioned equation, the three parcels presented represent the contribution of the wing, the vertical stabilizer and the wing-fuselage to the lateral stability.

$$C_{L_\beta} = \frac{dC_L}{d\beta} = (C_{L_\beta})_W + (C_{L_\beta})_{VS} + (C_{L_\beta})_{WF} \quad (8.8)$$

To have lateral stability, the right wing tip should rotate up in order to counteract a positive angle β , as represented in equation (8.9).

$$C_{L_\beta} = \frac{dC_L}{d\beta} < 0 \quad (8.9)$$

Taking into consideration the difficulty of accurately estimating the lateral stability coefficient for a conceptual aircraft, as a first approximation, one can consider equation (8.10), where $C_{n\beta}$ is the directional stability coefficient, presented in detail in section 8.3.

$$C_{L_\beta} = -C_{n\beta} \quad (8.10)$$

8.3 Directional Stability

The directional motion describes the rotational movement about the vertical axis. The directional stability coefficient is present in equation (8.11). This coefficient reflects the change the directional moment coefficient C_n suffers with respect to the slip angle (β) and takes into consideration three main influences - from the aircraft's fuselage, wing and vertical stabilizer.

$$C_{n\beta} = (C_{n\beta})_F + (C_{n\beta})_W + (C_{n\beta})_{VS} \quad (8.11)$$

In order to obtain directional stability, the directional stability coefficient must be positive, since a positive moment N will counteract the slide slip angle β . A positive directional stability coefficient also ensures a negative lateral stability coefficient, therefore providing lateral stability to the aircraft.

The contribution of the vertical stabilizer to the aircraft's directional stability is presented in equation (8.12).

$$(C_{n\beta})_{VS} = \bar{V}_{VS}(C_{L_\alpha})_{VS} \left(1 + \frac{d\sigma}{d\beta}\right) \frac{q_{VS}}{q} \quad (8.12)$$

The coefficient $\left(1 + \frac{d\sigma}{d\beta}\right) \frac{q_{VS}}{q}$ of equation (8.12) is presented in equation (8.13) and \bar{V}_{VS} in equation (8.14). In that same coefficient, z_W represents the position of the wing in height and h represents the height of the fuselage.

$$\left(1 + \frac{d\sigma}{d\beta}\right) \frac{q_{VS}}{q} = 0.724 + \frac{0.06S_{VS}/S_W}{1 + \cos\Lambda_{VS}} + 0.4 \frac{z_W}{h} + 0.009A_W \quad (8.13)$$

$$\bar{V}_{VS} = \frac{l_{VS}S_{VS}}{S_W b} \quad (8.14)$$

The value obtained for the $(C_{n\beta})_{VS}$ of the aircraft through the application of equation (8.12) is $0.272264 rad^{-1}$.

The contribution of the wing to the aircraft's directional stability is presented in equation (8.15), that gives a value of $0.00113766 rad^{-1}$ for $(C_{n\beta})_W$.

$$(C_{n\beta})_W = C_L^2 \left[\frac{1}{4\pi A} - \frac{\tan\Lambda}{\pi A(A + 4\cos\Lambda)} \left(\cos\Lambda - \frac{A}{2} - \frac{A^2}{\cos\Lambda} + 6\frac{x}{c} \frac{\sin\Lambda}{A} \right) \right] \quad (8.15)$$

The contribution of the fuselage to the aircraft's directional stability is presented in equation (8.16), where v constitutes the volume of the fuselage and h and w the height and the width of the fuselage, respectively. This computation gives a $(C_{n\beta})_F$ of $-0.09904 rad^{-1}$.

$$(C_{n\beta})_F = -1.3 \frac{v}{S_W b} \frac{h}{w} \quad (8.16)$$

Adding the contributions of the wing, the vertical stabilizer and the fuselage, the directional coefficient obtained is equal to 0.174363. This coefficient not only has a positive value, demonstrating that the aircraft is stable, but also is within the suggested interval of $0.08 \leq C_{n\beta} \leq 0.28$, as cited in [9].

9 Propulsion

The propulsion system is an essential element of the aircraft design. As mentioned previously this aircraft uses different means of propulsion for different mission segments: the aircraft will have an internal combustion engine to power a propeller for forward flight and four electric motors, each one powering two co-axial rotors, for vertical flight.

Therefore, in the next sections both a combustion and an electric motor will be selected, from those available on the market. In addition, the propeller's as well as the rotor's characteristics will be determined.

9.1 Vertical Flight

9.1.1 Electric Propulsion

As was stated above, an electric propulsive system will be used for vertical flight segments of the mission. Therefore, the electric motors must be able to comply with the requirements of the vertical take-off and landing.

Through the several iterations done when designing the aircraft, it was concluded that 8 rotors would be needed, due to constraints in the rotor radius size. It was then decided that the best approach would be for the aircraft to make use of four electric motors, where each one powers two co-axial rotors. The motors were chosen so that their combined power would not only be higher than the required by the aircraft, but would also result in a good design point, that is, it would provide the aircraft with a favorable power loading.

Taking all this into account, and after analyzing the electric motors commercially available (as shown in Table 9), the *MagniX magniDrive* electric motor was chosen, due to its high power, efficiency and flexibility. Each motor provides 170 kW of power, resulting in a total power of 680kW. The motor's specifications are present in the following table:

Table 8: *MagniX magniDrive* electric motor specifications [19].

Continuous Power	170 kW
Weight	12 kg
Diameter	562 mm
Length	74 mm

Table 9: Market study for electric motors [19].

	MagniX magniDrive	EMRAX 348	Siemens SP260D	MAGiDRIVE 300
Continuous Power	170 kW	210 kW	261 kW	240 kW
Weight	12 kg	42 kg	50 kg	45 kg
Diameter	562 mm	348 mm	418 mm	482 mm
Length	74 mm	105 mm	300 mm	200 mm
Specific Fuel Consumption	0.369 kg/kWh	0.525 kg/kWh	0.282 kg/kWh	0.412 kg/kWh

9.1.2 Rotor Design

With the electric motors chosen, the next step in the design is to determine the main characteristics of the aircraft's rotors. The Disk loading obtained was 891 N/m^2 . From this value the required total rotor area, A_t , can be computed using equation (9.1.2).

$$A_t = \frac{MTOW}{DL} \quad (9.1)$$

Given the MTOW value already discussed, we obtain a value of $25.12\ m^2$ for the total rotor area. Since the aircraft will have 8 equally-sized rotors, the required area of each rotor, A_r , is approximately $3.14\ m^2$.

From equation (9.1.2), it follows that the rotors have a radius of 1.00 m.

$$A_r = \pi R^2 \quad (9.2)$$

Rotor solidity, σ , is defined as the ratio of total blade area to the disk area of the rotor, and is therefore given by the following equation, where, in addition to the parameters already discussed, N is the number of blades in each rotor and c is the mean blade chord:

$$\sigma = \frac{cRN}{A_r}. \quad (9.3)$$

Rotor solidity for conventional helicopters has typical values between 0.07 and 0.12. Historically, a rotor solidity of 0.1 is the most employed, hence we will assume this value for our design. Moreover, a value of 6 blades for each rotor was chosen, in order to reduce the amount of noise generated during hover, at the cost of induced drag. With that in mind, from equation (9.1.2) results that the mean blade chord is 5.2 cm. To summarize, the main rotor characteristics can be found in Table 10.

Table 10: Rotor characteristics.

Number of rotors	8
Number of blades per rotor	6
Rotor diameter	2 m
Mean blade chord	5.2 cm

9.2 Forward Flight

9.2.1 ICE Propulsion

ICE propulsion will be used for forward flight, which is majorly composed by the cruise segments of the proposed mission, the conditions of which are present in Table 11.

In order to reduce costs and minimize design problems and early design stage uncertainties, it was decided to use an existing engine instead of developing a new one. Taking into consideration the low value of the Mach number in cruise, it was considered choosing between a piston engine and a turboprop. The latter is a better solution since it has a higher T/W, higher possible operational altitudes and lower vibration levels, being appropriate for mid-range commuter aircraft.

When iterating for a favourable design point, the power required for the horizontal flight was taken into consideration, having a value of 372 kW been chosen. This value reflects a previous market research of motors, present in Table 12, used in aircraft performing similar mission profiles. Attending all the requirements related to the cruise conditions, the geometry and the dimensions of the aircraft, Rolls-Royce's M250-C28B motor, whose specifications are present in Table 13, was chosen to be used in the forward flight segments of the mission.

Table 11: Cruise conditions.

Altitude	1500 m
Cruise Speed (V_{cruise})	84 m/s
Mach at cruise (M_{cruise})	0.25
Air density (ρ)	1.056 kg/m ³
Speed of sound (a)	334.55 m/s

Table 12: Market study for ICE propulsion [20].

	Rolls-Royce M250-C28B	TP100 (x2)	Vedeneyev M14P	Rolls-Royce RR500
Continuous Power	373 kW	160 kW	268 kW	280 kW
Dry Weight	103.9 kg	61.6 kg	214 kg	102 kg
Diameter	846 mm	398 mm	985 mm	590 mm
Length	1219 mm	891 mm	924 mm	1090 mm
Specific Fuel Consumption	0.369 kg/kWh	0.525 kg/kWh	0.282 kg/kWh	0.412 kg/kWh

Table 13: Rolls-Royce M250-C28B motor specifications [20].

Continuous Power (P)	373 kW
Maximum Rotational Speed (n)	6016 rpm
Dry Weight	103.9 kg
Diameter	846 mm
Length	1219 mm
Specific Fuel Consumption	0.369 kg/kWh

9.2.2 Propeller Design

From the values of the power loading for the horizontal flight and the MTOW obtained in the design point, the power required for the horizontal segments of the mission is 372 kW.

The value of the rotational speed present in Table 13 is the maximum rotational speed that this ICE engine can provide. Thus, it should not be the value used in the calculations, since the engine will be operating with its continuous rotational speed, not its maximum one. The value of the continuous rotational speed of this particular engine is not provided by its producer, thus having a value of 2080 rpm been estimated, through a computation of the average of the values of a market study of engines with similar characteristics.

A value of 0.7 for the M_{tip} was assumed, in order to avoid the compressibility effects at the tip of the blades of the propeller. The tip velocity is 234.14m/s, since $V_{tip} = M_{tip} \times a$. Applying equation (9.4), for the calculation of the V_{tip} at the cruise segments, a value of $nD = 69.57$ is obtained. From this, one can obtain a value of 2m for the diameter of the propeller (D).

$$V_{tip} = \sqrt{(n\pi D)^2 + V_{cruise}^2} \quad (9.4)$$

The advance ratio, J , and the power coefficient, C_P are given by equations (9.5) and (9.6), respectively.

$$J = \frac{V_{cruise}}{nD} = 1.2 \quad (9.5)$$

$$C_P = \frac{P}{nD} = 0.26 \quad (9.6)$$

Given these J and C_P , figure 37 can be used to estimate an ICE motor efficiency of 80% and a $\theta_{3/4}$ of 37° .

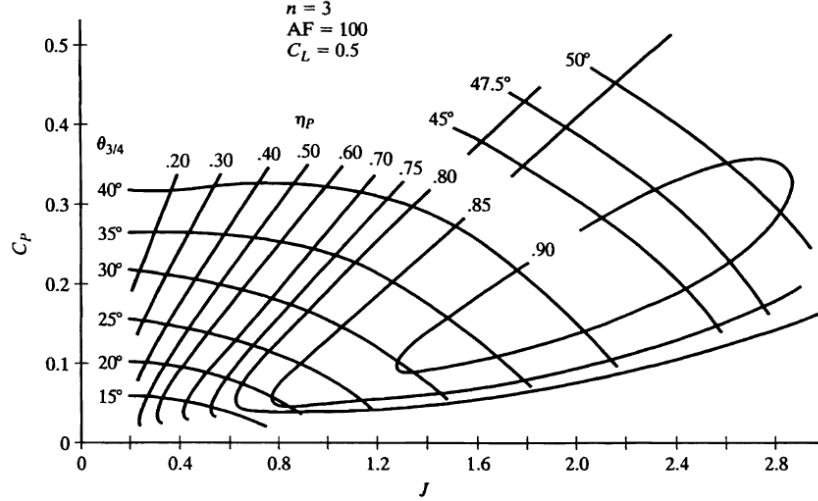


Figure 37: Sample propeller efficiency for forward flight (three blade propeller) [9]

Through equation (9.7), the value of the thrust needed for forward flight can be obtained.

$$T_{av} = \frac{P\eta_P}{V} = 3552N \quad (9.7)$$

9.3 Propulsive Architecture

The hybrid-electric system present in the aircraft (which comprises the ICE motor, the electric motors and the batteries) can be divided in two subsystems: one for vertical flight and one for forward flight, since the batteries will not need recharging during flight for the proposed mission.

The vertical and horizontal flight propulsive architectures are represented in Figures 38 and 39, respectively.

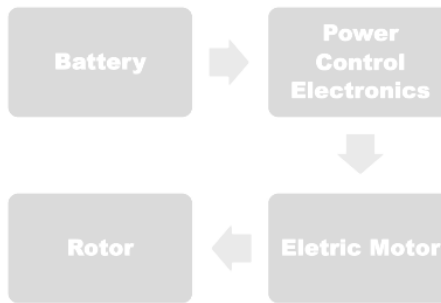


Figure 38: Propulsive architecture used in vertical flight.



Figure 39: Propulsive architecture used in forward flight.

10 Emissions

Our Urban Air Mobility aspirations face a challenge. Our current technology isn't well suited for operation in an urban environment. Helicopters, as the only realistic option due to their VTOL capabilities, are not suited for urban areas where low noise and low pollutant emissions are a priority. Hence, the true importance and significance of this study on UAM vehicles lies in this section, because minimizing the noise and pollutant emissions inside urban environments is the distinctive and interesting design goal of this category of hybrid-electric VTOL aircraft.

To guide the execution in the right direction to achieve that goal, two general requirements were established. First, the noise perceived by an observer 500 ft away from an hovering aircraft should not exceed 70 dB. Secondly, the design should minimize the equivalent CO₂ emissions generated by an operating aircraft, considering the impact of its full life cycle. These requirements should be perceived as guidelines for the design study performed.

10.1 Noise

One of the known disadvantages of the concept chosen, in section 2 of this study, was the noise it generated in flight, especially worrisome during vertical take-off and landing. The aircraft's propulsion system is the main responsible, despite its quiet electric motors. The problem lies in its four pairs of coaxial rotors, which generate noise while rotating at high speeds inside the atmosphere.

To mitigate this issue, two design decisions were employed:

- The tip speed of the rotor blades, V_{tip} , is limited to Mach 0.4;
- The number of blades, N , in each rotor was increased to 6.

The highest the tip speed, the louder the rotating blades will be. However, limiting or decreasing the rotation speed of the rotors must be compensated in another way, since slower rotating blades generate less lifting force. That is the justification for increasing the number of blades to six per rotor, so as to maintain the thrust while generating less noise.

Following the proposed semi-empirical models for rotational and vortex noise [17] and using an adapted version of the provided MATLAB code, it is possible to compute the Sound Pressure Level (SPL) at a distance of 500 ft from the hovering aircraft. The model only accounts for rotor related noise and considers the presence of an *hover out-of-ground effect*, which indicates the production of higher noise levels.

The MATLAB code needs, as input, information about the number of rotors, as well as the number of blades, N , in each of them, V_{tip} in m/s, the radius of the rotors' blades, their thickness and chord, the rotor solidity, σ , the aircraft's MTOW and the electric motor power output.

The output is the total sound pressure level generated and, using the data previously determined on sections 9.1.1 and 9.1.2 and a maximum blade thickness of 12%, the output turns out to be

$$\text{SPL (at 500 ft)} = 74.16 \text{ dB}$$

which means that the 70 dB requirement is nearly met. As such, considering also that the model disregards other possible sources of noise, this analysis serves only as a first approximation and the task of lowering the noise level further is left for future work, using CFD or other tools which more easily can improve this aspect of the vehicle.

10.2 Pollutant Emissions

Besides noise pollution, the air quality is also a major concern in large cities and certainly transportation is one of the major contributors to that issue. By using its internal combustion

engine only above a certain altitude, sometime after take off, the UAM vehicle proposed here could minimize the presence of green house gases and other particles at ground level, thus improving the air quality.

Since most of the information regarding electric aircraft production and disposal isn't yet fully known, some of the aspects related to this were not studied. As such, the sources of CO₂ equivalent emissions considered comprised battery production, battery charging and fuel consumption.

As proposed in the project guidelines, for the purpose of this study, the battery technology considered should be state-of-the-art. This means the batteries used for the electric propulsion system can have a specific energy density of up to 300 Wh/kg. Assuming this and according to the mission flight profile, a battery pack mass of 152 kg is required to complete the mission and meet the remaining requirements. A reserve of 20% is already included in that mass value.

Now, according to [21], Lithium Sulfur (LSB-Li) batteries will have specific energy densities close to the aforementioned proposed value, so those were the ones considered here. These batteries feature a maximum of 714 life cycles and the lower pollutant emissions related to their production of all the battery types studied. Considering all the CO₂ equivalent sources though, the battery production amounts to just 1% of the total emissions, as can be seen in Figure 40.

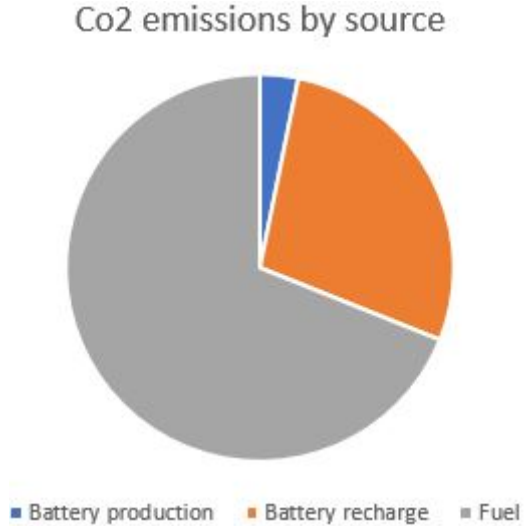


Figure 40: Distribution of the total CO₂ equivalent emissions by source for the lifetime of each UAM aircraft.

Battery recharge, however, needs electricity which often is not from fully renewable sources. To estimate the emissions coming from the electricity consumed in the recharging of the batteries, the computation performed in the MATLAB code considers the average CO₂ equivalent emissions per unit of energy produced in the European Union, which was 295.8 gCO₂/kWh in 2016. [17]

Regarding the fuel consumed in the vehicle's combustion engine, using the most efficient fuel in the market, in terms of CO₂ emissions per kWh, lowers the pollutant emissions considerably. Although it is an average fuel in terms of specific energy per mass, this is not an issue because the fuel mass in the vehicle is quite small to actually make a relevant impact.

All in all, the aircraft is estimated to emit a total of 34.56 tonnes of CO₂ during its lifetime, which, divided by the estimated number of missions, amounts to about 48.4 kg per mission or approximately 240 gCO₂/km. For comparison, this is just twice the emissions of an average car sold in the EU in 2019. [22]

11 Cost Analysis

To estimate the life-cycle cost of the aircraft developed throughout this work, a top-down cost analysis model is used, as this is simply the conceptual design stage of the aircraft.

The model used in this work presents empirical relations based on a methodology presented by the RAND corporation in 1986 [17]. This model is heavily dependent on the aircraft's top speed and available empty weight, and divides the life-cycle cost in four different parts:

1. Research Cost
2. Development, testing and evaluation cost
3. Acquisition/Production cost
4. Operations and Management cost

11.1 Development, testing, evaluation and production

For this section it is important to note that the empirical formulas produce the hours needed for the different kind of work required to develop a transport aircraft. For the context of this model, only four different categories are considered:

- Airframe Engineering;
- Tooling;
- Manufacturing Labor;
- Quality Control.

After the hours needed to produce the aircraft are known, the numbers are multiplied by the average hourly wage for the different categories in order to obtain the cost of each part.

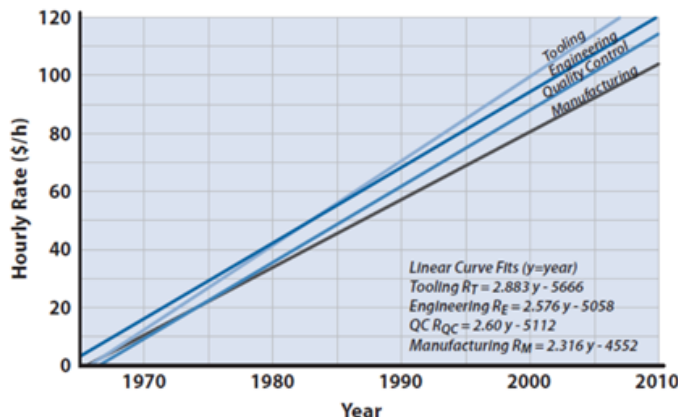


Figure 41: Hourly wage empirical extrapolation, based on the value of 1998 USD [17]

To calculate the hourly wage for each category, an extrapolation of the wage values over the years is obtained from the RAND study (Figure 41), in relation to the dollar price in 1998. As such, the values need to be multiplied further on by the Consumer Price Index (CPI) of the current year.

Using the interpolation for the year of 2020, the hourly wages are obtained.

As for the calculation of the hours needed for development and production, those are calculated by the formulas in Table 15, also from the study, in which AEW is the available empty

Table 14: Obtained values for hourly wages for the different categories

Category	Hourly rate (\$/h)
Airframe Engineering	145.52
Manufacturing Labor	126.32
Tooling	157.66
Quality Control	140.00

Table 15: Empirical relation for the work hours needed

Category	Equation
Airframe Engineering	$E = 4.86 (AEW)^{0.777} V_{max}^{0.894} Q^{0.163}$
Manufacturing Labor	$L = 7.37 (AEW)^{0.82} V_{max}^{0.484} Q^{0.641}$
Tooling	$T = 5.99 (AEW)^{0.777} V_{max}^{0.696} Q^{0.263}$
Quality Control	$QC = 0.13L$

weight (in lb), V_{max} is the top speed (in m/s) and Q is the number of produced units in a certain phase.

In addition to the basic cost of those main categories, there are also costs specific to each design phase.

11.1.1 Development, Testing and Evaluation

Specifically, for the DT&E phase, additional costs need to be considered:

- Development support;
- Flight test operations;
- Manufacturing Material and Equipment.

The development support cost encompasses nonrecurring manufacturing effort to aid engineering tasks, such as test items, parts and mock-ups. The more innovative the aircraft, the higher the cost. For the purpose of this work, the empirical formula from the RAND study is used:

$$C_{DS} = 66 (AEW)^{0.63} V_{max}^{1.3} \quad (11.1)$$

The flight test operations aim to assert the qualities of the developed aircraft with different tests, for example of its handling capabilities. The cost associated with this process can be estimated by the formula:

$$C_{FT} = 1852 (AEW)^{0.325} V_{max}^{0.822} Q^{1.21} \quad (11.2)$$

Lastly, the manufacturing material and equipment encompasses the estimation of all the raw material and purchased parts for the duration of DT&E. These can be approximated by:

$$C_{MME} = 16.39 (AEW)^{0.921} V_{max}^{0.621} Q^{0.799} \quad (11.3)$$

In conclusion, and using only $Q = Q_d = 5$ aircrafts for the DT&E part, the costs are summarized in Table 16.

Table 16: Top down cost of the DT&E phase

Category	Cost (millions of USD 1998)
Airframe Engineering	28.6
Manufacturing Labor	19.5
Tooling	18.3
Quality Control	2.80
Development support	3.55
Flight test operations	6.92
Manufacturing Material and Equipment	1.86
Total	82.1

Table 17: Top down cost of the Acquisition/Production phase

Category	Cost (millions of USD 1998)
Airframe Engineering	8.58
Manufacturing Labor	35.1
Tooling	9.97
Quality Control	6.82
Engines	1.35
Manufacturing Material and Equipment	5.62
Total	67.5

11.1.2 Acquisition/Production

In this stage of the project cycle, the product is complete and ready to be produced.

The same equations for the hours required for this part of the project cycle stay the same as in the previous part, however, it is not as simple as using the number of production units.

Given $H(Q)$ the generic function for the hours required for any of the main four categories in function of the number of units, the number of hours for the production stage are given by:

$$H_p = H(Q_p + Q_d) - H(Q_d) \quad (11.4)$$

Where Q_p are the production units and Q_d are the development units. In addition to this, additional costs need to be considered:

- Manufacturing Material and Equipment
- Engine costs

The material equipment costs are estimated using equation (11.3) and the engine costs were converted to what they would have been in 1998, dividing by the CPI. The engine cost are the values in the market study.

It was assumed that there would not be any cost associated to the opening of a new manufacturing and production facility.

For a fleet of $Q_p = 20$ units, the costs are summarized in Table 17.

11.2 Operations and Maintenance

The cost of operations and maintenance are a big part of the total cost. It encompasses all the variables necessary to maintain the operation, such as crew salary, maintenance cost and fuel and oil cost.

The main O&M cost can be separated into three categories:

- Fuel, oil and lubricant
- Crew
- Maintenance personnel

The RAND model also provides empirical relations for one year of operations, divided into those three parts.

The cost of the fuel, oil and lubricant is given by the following expression:

$$C_F = 1.05 \frac{W_f}{t_m} FH \frac{F}{3.79\rho_k} N_A \quad (11.5)$$

Where W_f is the fuel weight per mission, t_m is the mission time, FH is the number of flying hours per year, F is the jet fuel price, N_A is the fleet size and ρ_k is the density of kerosene.

The cost associated with the crew is:

$$C_C = C_S \cdot CR \cdot N_A \cdot FH \quad (11.6)$$

Where C_S is the crew salary (\$/h/year) and CR is the number of crew members per aircraft. Lastly, the cost associated with the maintenance personnel is given by:

$$C_{MP} = M_S \cdot FH \cdot N_A \cdot MMH/FH \quad (11.7)$$

Where M_S is the maintenance personnel salary (\$/h/year) and MMH/FH is the proportion of maintenance hours for each flying hour.

The previous expressions calculate the cost of each part of the O&M stage per year, so for a multiple year operation, a simple multiplication is needed.

For this project, an operation time of 10 years was set.

The constants used for this part of the work are all in Table 18.

Table 18: Constants used for the O&M Cost calculation

Fleet size (N_A)	10 units
Flying hours (FH)	1638h (4 missions of 1.122h per day, per year)
Crew Salary	102870/FH = 62.8\$/h/year [17]
Maintenance personnel salary (M_S)	32.4 \$/h/year [17]
Jet fuel price (F)	1.406 \$/gallon [17]
Crew number (CR)	1 pilot
Fuel Weight (F)	26.38 kg
Maintenance hours ratio (MMH/FH)	8
Time of mission (t_m)	1.122 hours

As a result, after a ten-year period, the O&M costs are summarized in Table 19.

Table 19: Top down costs for O&M phase for ten years of operation

Category	Cost (millions of USD 2020)
Fuel	4
Crew Cost	21
Maintenance Personnel	85
Total	110 million USD 2020

11.3 Research cost

The last point that needs consideration is the cost of research, which is not included in the formulas for the development, testing and evaluation. Upon conferencing with Professor Afzal Suleman about the issue, it was decided that the research cost would be approximately that of 10% of the remaining cost. As such the cost of research can be given by:

$$C_r = 0.1 \cdot (CPI \cdot (C_{DTE} + C_P) + C_{OM}) \approx 35 \text{ million USD} \quad (11.8)$$

11.4 Total top-down approximate cost

After all the calculations, and adjusting the values to the US dollar value as of December 2020, ($CPI = 1.5877$, [23]), the costs are distributed as such:

Table 20: Top down cost overview

Category	Cost (Millions of US dollars 2020)
Research	35
DT&E	130
Production	107
O&M	110
Total	382 Million USD 2020

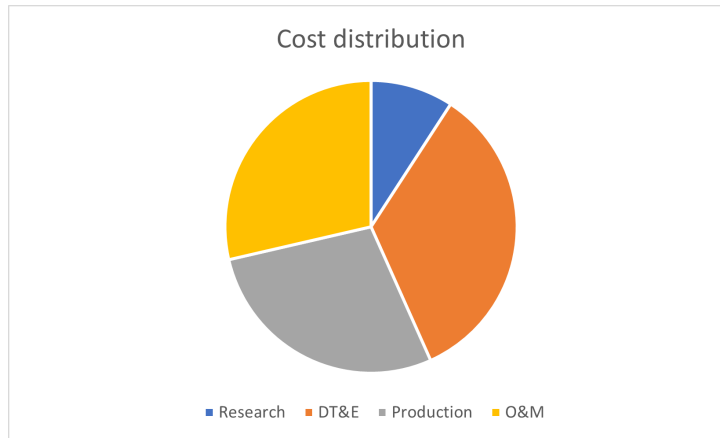


Figure 42: Total top down cost pie chart

The unitary price for the aircraft, without accounting for any sort of profit, is the following C_u :

$$C_u = 5.35 \text{ million USD (2020)}$$

This value, while quite high, is heavily dependant on the number of aircrafts produced. As the price isn't linear with this number, a higher number of production units would lead to a lower unit price. For example, increasing the number of production units to 200 instead of 20 would lead to a unitary cost of only 2.48 million USD (2020).

12 CAD Model



Figure 43: CAD image of the final aircraft design (side view)



Figure 44: CAD image of the final aircraft design (front view)

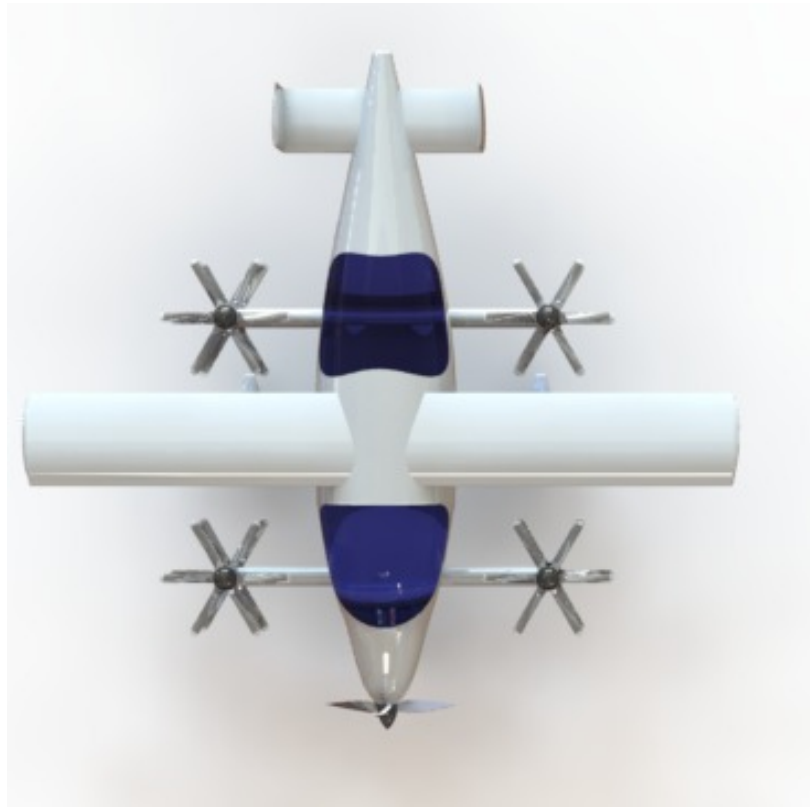


Figure 45: CAD image of the final aircraft design (top view)

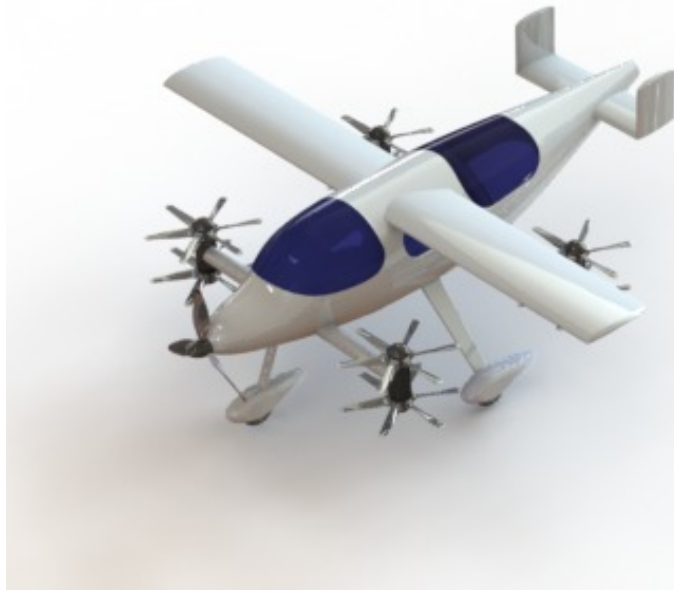


Figure 46: CAD image of the final aircraft design (isometric view)

13 Conclusion

The aircraft designed meets all the requirements, except for the SPL at 500 ft constraint. Despite of this, its design emphasized versatility and simplicity, thus taking full advantage of a VTOL design.

Its versatility is nowhere clearer than in its operational possibilities: the aircraft is capable of multiple vertical segments inside a 300 km range, even with high transition altitudes, when compared to other similar designs. The aforementioned focus on simplicity is part of the reason a fixed wing VTOL design was chosen: a fixed wing is much cheaper to develop, maintain and manufacture, than a tilted one. Moreover, using four engines for vertical flight and one for horizontal flight ensures redundancy, while also being cheaper to develop and maintain than a tilt rotor configuration.

This design philosophy was also applied to the initial aircraft sizing: the design point constraints were chosen to ensure the aircraft can perform missions with even more stringent constraints than those it was designed for. Furthermore, the wing and rotor area were chosen flexibly, allowing the aircraft to fly with even more weight, or in other, more demanding mission profiles.

Regarding the aerodynamic design, priority was given to designing a wing that performed very well at low speeds, since VTOL aircraft need to be able to generate high lift at low speeds when transitioning from vertical to horizontal flight. The wing's 3D design is another example of simplicity and practicality: taking the cue from other small general aviation designs, a rectangular wing with no sweep or dihedral angle were chosen. While not as aerodynamically efficient as tapered and swept wings, this aircraft's wing is at least conceptually cheaper to produce. As for its aerodynamic drawbacks, they can be easily corrected using more economically means. Moreover, a H-tail was chosen for the good control ability it provides at low speeds.

The fuselage designed is highly versatile, as it can accommodate several configurations: passenger transport, cargo delivery and air ambulance. Additionally, the cargo door and rail system designed ensures a quick and easy way of changing configurations and refurbishing the aircraft. As for its structural design, a handful of analysis were conducted, including flight envelopes and the shear stress and bending moment diagrams for the wing and fuselage.

The aircraft is directionally, laterally and longitudinally stable, despite of the simple rectangular wing + tail configuration chosen. Its stability coefficients are well inside their appropriate ranges, and the static margin is the 10% for all the configurations. Furthermore, given the relatively low amount of fuel used per mission, the aircraft's stability differs very little during each flight, negating the need to use costly fuel pump designs to maintain longitudinal stability.

As aforementioned, the propulsion system was designed with simplicity and mission versatility in mind: whilst using eight rotors may seem complex, using 4 pairs of co-axial rotors is by and large simpler than using several tilt rotors (it goes without saying that it is also simpler than rotating the whole wing). Additionally, using 4 engines also ensures redundancy, and less emissions, since less powerful electric engines are much more efficient and lighter than more powerful ones. The rotor area was chosen to ensure the aircraft is able to perform vertical segments with a much larger weight, to ensure very high level of safety. As for the horizontal mode propulsion system, a simple ICE turboprop + propeller configuration was selected: it is an efficient, tried and tested choice, which easily meets the design requirements for this design.

Noise and CO_2 emissions are arguably the biggest drawback for this, and many other eVTOL designs. Any aircraft operating in an urban scenario has to meet stringent noise emission requirements, however, eVTOL designs are notorious for their liberal use of propellers and rotors, which make meeting that requirement an herculean task. Furthermore, whilst lithium batteries and electric propulsion in general have taken huge leaps forward since the 1980's, full-electric commercial aircraft are decades away, even assuming the industry is interested in pursuing it as goal. Thus, this design utilizes and hybrid propulsion system, which, while performing well in general, does mean that the ICE engine is responsible for more than half of the total CO_2 emissions. Notwithstanding, this design is similar to an average car when it comes to CO_2 emissions per km.

A cost analysis was also performed, however, the novelty and unorthodoxy of eVTOL designs difficult any assessment of their potential costs. Using Formulae used to estimate the cost of

large aircraft designed decades ago are by no metric a good method to apply to this aircraft, even still, they are the best one there is. It is also worth mentioning that given the group's focus on simple and cost effective components, the project's cost should be significantly lower than other project's with tilt rotors or wings, or more complex wing designs.

To conclude, the final design of this aircraft is able to meet all the requirements with flying colors, however, it is clear that any type of eVTOL design faces many practical challenges: namely, a high operation cost, low passenger volume and relatively high CO_2 emissions when compared to boats, trains and buses. Moreover, this modest decrease in CO_2 emissions, when compared to a fully ICE design, is achieved at a very high cost, both financially and design wise.

References

- [1] AirCanada. Our Fleet. <https://www.aircanada.com/ca/en/aco/home/fly/onboard/fleet.html>. [Last accessed 18/10/2020].
- [2] De Havilland Canada DHC-3 Otter. <https://www.airliners.net/aircraft-data/de-havilland-canada-dhc-3-otter/179>. [Last accessed 18/10/2020].
- [3] Longranger 206L-3. <https://www.globalair.com/aircraft-for-sale/Specifications?specid=312>. [Last accessed 18/10/2020].
- [4] Boeing Personal Air Vehicle. <https://qodebrisbane.com/boeing-personal-air-vehicle-successfully-tested-when-will-you-see-air-taxi-in-your-city/>. [Last accessed 18/10/2020].
- [5] City Airbus eVTOL Prototype Makes First Flight in Germany. <https://www.rotorandwing.com/2019/05/03/city-airbus-evtol-prototype-makes-first-flight-in-germany/>, . [Last accessed 18/10/2020].
- [6] Airbus CityAirbus. <https://evtol.news/airbus-helicopters>, . [Last accessed 18/10/2020].
- [7] JobyAviation. <https://www.jobyaviation.com/>. [Last accessed 18/10/2020].
- [8] Lilium Jet. <https://evtol.news/lilium/>. [Last accessed 18/10/2020].
- [9] T. C. Corke. *Design of Aircraft*. Pearson Education, 2003. ISBN 0-13-089234-3.
- [10] D. P. Raymer. *Aircraft Design: A Conceptual Approach*. AIAA Education Series, 2nd edition, 1992. ISBN 0-930403-51-7.
- [11] TU Delft. Fuselage Design. Aerospace Design and Systems Engineering Elements I course notes.
- [12] M. H. Sadraey. *Aircraft Design: A Systems Engineering Approach*. John Wiley & Sons, 2013. ISBN 978-1-119-95340-1.
- [13] Cessna 172S. <https://cessnaowner.org/172-skyhawk/>. [Last accessed 06/12/2020].
- [14] L. O'Rourke. The Mathematics of Simple Beam Deflection.
- [15] FAA. Federal Aviation Regulations - Part 25 - Airworthiness Standards: Transport category airplanes. Subpart C - Structure, .
- [16] FAA. Federal Aviation Regulations - Part 23 - Airworthiness Standards: Normal, utility, acrobatic and commuter category airplanes. Subpart C - Structure, .
- [17] Course slides. <https://fenix.tecnico.ulisboa.pt/disciplinas/PAer577/2020-2021/1-semestre/2—lectures-powerpoint-presentations>. [Last accessed 10/12/2021].
- [18] V. de Brederode. *Aerodinâmica Incompressível: Fundamentos*. IST, 4th edition, 2014. ISBN 9789898481320.
- [19] Products Magnix. <https://www.magnix.aero/products>. [Last accessed 15/12/2020].
- [20] Civil Turboshaft/Turboprop Specifications. <https://www.jet-engine.net/civtsspec.html>. [Last accessed 15/12/2020].
- [21] S. P. M. et al. Life cycle engineering of future aircraft systems: the case of evtol vehicles. *Procedia CIRP*, 90:297–302, 2020.

- [22] EEA. Average co2 emissions from newly registered motor vehicles in europe. <https://www.eea.europa.eu/data-and-maps/indicators/average-co2-emissions-from-motor-vehicles/assessment-2>. [Last accessed 9/01/2021].
- [23] BLS. <https://www.bls.gov/cpi/>. [Last accessed 18/12/2020].